Effect of tunable composition-shape of bio-inspired Pt NPs electrocatalyst in direct methanol fuel cell: Process optimization and kinetic studies

Nurul Atiqah Izzati Md Ishak[a,b,*], Siti Kartom Kamarudin[b,c,*], Muliani Mansor[d], Norilhamiah Yahya, Raihana Bahru, Saidur Rahman[a,e]

[a]*Research Centre for Nano-Materials and Energy Technology (RCNMET), School of Engineering and Technology, Sunway University, Bandar Sunway, Petaling Jaya, 47500, Selangor Darul Ehsan, Malaysia*
[b]*Fuel Cell Institute, Universiti Kebangsaan Malaysia, 43600 UKM Bangi, Selangor, Malaysia*
[c]*Department of Chemical and Process Engineering, Faculty of Engineering and Built Environment, Universiti Kebangsaan Malaysia, 43600 UKM Bangi, Selangor, Malaysia*
[d]*Malaysia-Japan International Institute of Technology, Universiti Teknologi Malaysia Kuala Lumpur, Jalan Sultan Yahya Petra, Kuala Lumpur 54100, Malaysia*
[e]*School of Engineering, Lancaster University, Lancaster, LA1 4YW, UK*

**Email: ctie@ukm.edu.my, atiqahmi@sunway.edu.my*

ABSTRACT

Highly efficient bio-inspired platinum nanoparticles (Pt NPs) as an electrocatalyst with superior intrinsic kinetics and high performance for methanol oxidation reaction (MOR) derived from green synthesis of bio-waste utilization is of great interest. The bio-inspired Pt NPs were examined for their kinetic parameters in terms of the Tafel plot, exchange current, square root of the scan rate, methanol diffusion coefficient, activation energy (E_a), and factors influencing current density. Bio-inspired Pt NPs exhibit a fast kinetic reaction with a low Tafel value of 179 mV dec^{-1} and exchange current, $\alpha = 0.33$, compared to commercial Pt black (233 mV dec^{-1}, $\alpha = 0.25$). The bio-inspired Pt NPs display low activation energy, Ea, as the potential increases, indicating improved intrinsic kinetics, and the MOR catalyzed by bio-Pt NPs was discovered to be a diffusion-controlled process. The parametric effect of bio-inspired Pt NPs concentration has a crucial influence on the anisotropic morphological structure and interconnection to the current density (mA mg^{-1}) of MOR. Central Composite Design (CCD) was applied for RSM-based modeling and analyzing the parameter effects, including bio-inspired Pt NPs concentration, methanol concentration, and electrocatalyst loading to optimize the current density. The optimized current density produced by bio-inspired Pt NPs was 640.11 mA mg_{Pt}^{-1} at ideal conditions of 1.5 mM bio-Pt NPs, 1.05 M CH_3OH, and 2.14 mg. Ultimately, the passive DMFC single-cell powered by bio-inspired Pt NPs generates power density with Pmax of 5.70, 6.67, and 8.28 mW cm^{-2} at 25, 80, and 100 ^oC. Thus, bio-inspired Pt NPs derived from green synthesis pathways and biomass-mediated extract have been proven to be viable and sustainable anode electrocatalysts for utilization in the energy conversion of renewable energy with outstanding performance.

Keywords: Green synthesis; materials chemistry; Methanol oxidation reaction; Direct methanol fuel cell; biomass utilization

1. INTRODUCTION

The energy crisis and the need for clean energy to sustain the environment have necessitated the development of alternative renewable energy sources to replace the finite supply of non-renewable fossil fuels and overcome their harmful environmental effects. Direct methanol

fuel cells (DMFCs) are a possible solution to alleviate energy problems and obtained extreme attention due to their high energy density, low-carbon emissions, easy handling, and portable wise (Kamarudin and Hashim, 2012), (Zhang et al., 2016). DMFCs are electrochemical energy devices that transform chemical energy from methanol (fuel stock) into electrical energy cleanly and efficiently, with potential applications in electric vehicles and mobile power sources (Shaari and Kamarudin, 2018). Platinum (Pt) and platinum-based nanomaterials are regarded as state-of-the-art and exceed applied in many energy conversion reactions due to their high catalytic efficiency for electro-oxidation reactions, highly excellent electrooxidative materials and high specific surface area (Wo et al., 2023), (Mohamed et al., 2016). Despite having great working catalysts, Pt has several downsides that prevent the market acceptance of DMFCs, including scarcity, high cost, easy CO poisoning effect, and sluggish kinetics (Yao et al., 2021). The advancement of DMFC technology requires a highly active electrocatalyst to reduce the overpotential due to the sluggish kinetic reaction of anodic methanol electro-oxidation, which correlates with the structure, morphologies, materials, and synthesis methods that play a considerable role in the effectiveness of catalyst performance (Du et al., 2013).

Innumerable efforts have been made to produce a catalyst with high catalytic efficiency, including the discovery of new catalysts, morphology and size adjustments, the inclusion of support, alloying with various noble and non-noble metals, and the addition of dopants to the materials (Chen et al., 2020). However, researchers are also searching for novel preparation routes (Chen et al., 2020). The development of new, practical, and risk-free green synthesis techniques has been mandated by the principles of green chemistry due to the growing need to avoid employing chemicals that pose a threat to the environment. Due to their eco-friendly practices, biocompatibility, affordability, lack of harmful reagents, simplicity, and scalability, green synthesis methods have recently gained prominence as a

substitute for traditional physical and chemical synthesis. The biosynthetic process works similarly to conventional chemical reduction, except that expensive, toxic, and dangerous reagents such as N, N-dimethyl formamide (DMF), sodium borohydride, hydrazine, block copolymers, and Tollens reagents are replaced by natural plant extracts to synthesize nanoparticles. Plant extracts contain a diverse range of bioactive organic molecules, including alkaloids, proteins, polyphenolics, and flavonoids, which are made up of a variety of functional groups that reduce metal ions to metal nanoparticles in a single step in an ambient condition (Mittal et al., 2013), (Dauthal and Mukhopadhyay, 2016).

Although research on the use of materials derived from biosynthesis, particularly in the study of electrochemical energy conversion, is still in its infancy, it has been established that these materials are superior catalysts. These bio-inspired materials, which are synthesized from agricultural waste and employed as reducing agents in the chemical reduction process, have shown remarkable efficiency and stability in various electrochemical reactions, such as alcohol oxidation reactions, hydrogen evolution reactions, and oxygen evolution reactions (Nayak et al., 2022), (Velázquez-Hernández et al., 2020), (Fuku et al., 2019), (Guo et al., 2019), (Selvanathan et al., 2023), (Darabi et al., 2023). As a result, they hold great potential for revolutionizing energy conversion technologies and reducing reliance on traditional catalysts derived from non-renewable resources. Similarly, this study created Pt NP electrocatalysts using sugarcane (*Saccharum officinarum L.*) bagasse extract as a reducing agent for efficient MOR activity. Numerous parameter variables, including catalyst concentration, catalyst loading, molar ratio of catalyst to support, etc., have an impact on electrocatalyst performance to operate at high current densities. Response Surface Methodology (RSM) modelling is used to statistically identify the major components that lead to the high electrocatalytic activity since the green biosynthesis procedures have a substantial impact on the performance of the bio-inspired Pt NPs as an electrocatalyst. The

utilization of the RSM based on the central composite design (CCD) approach facilitates a more comprehensive assessment of the significance of individual factors and their interrelationships with the designated response variable (Balajii and Niju, 2019). Kivrak et al., (2018), proposed RSM based on the CCD model to optimize the current density of the Pd electrocatalyst in the formic acid oxidation reaction, which includes catalyst loading, $NaBH_4$ reducing agent concentration, water volume, and reaction time. Yahya et al., (2017) determined the factors of NaOH electrolyte concentration and operating temperature for the response of current density (mA/cm^2) in the glycerol oxidation by PdAu/VGCNF. The study of Karim et al., 2017 using cobalt phthalocyanine/carbon-tungsten oxide nanowires ($W_{18}O_{49}$) demonstrated investigation of several parameters for optimization such as pyrolysis temperature, mass ratio of CoPc/C to C:WCl_6 and synthesis method, to the responses of oxygen reduction reaction (ORR) activities. In applying the methanol oxidation reaction (MOR), Abdullah et al., (2020) reported that a statistical model predicted the following optimized conditions: 78.90% MXene composition, 19.71% Nafion content, and 2.82 M methanol concentration, which is the maximum current density produced by the PtRu/Mxene. In this context, changes in any of the variables leading to the need to significantly improve methanol oxidation reactions both in the synthesis method and during methanol partial oxidation cell operation are acceptable for further study. The previous findings served as a foundation for conducting an optimization analysis of the reaction parameters involved in the process of methanol oxidation for this study.

To better understand the fundamentals of the bio-inspired Pt NPs catalytic behaviors, kinetic studies in MOR are conducted. Research on electrochemical kinetics holds significant importance in the realm of fuel cell operation. There is an extensive amount of literature on the topic of kinetics. For instance, Javan et al., 2019 conducted a study that explored the electrochemical kinetics of Pd NPs supported by reduced carbon quantum dots in MOR.They

extracted the kinetic parameters from cyclic voltammetry (CV) and Tafel plots, and it was found that a higher active surface area of the catalysts can produce higher kinetic catalytic activity due to lower diffusion polarization. Douk et al., (2018a) fabricated bimetallic platinum-silver NPs supported on graphene (Pt-Ag/G) catalysts for methanol oxidation. They study the kinetic performance of MOR by using CV with different scan rates. It is found that the higher sweep rate enhances the oxidation peak of methanol and shifts the peak potential of MOR to a more positive value. The current versus $\upsilon 1/2$ plot shows a linear increase in oxidation peaks with the scan rate, indicating that mass transport controls the MOR. Herein, this work aims to evaluate the effect of the catalyst concentration, catalyst loading, and methanol concentration on the current density (mA/mg_{Pt}) of bio-inspired Pt NPs in MOR by assessing it using one-factor-at-a-time (OFAT) and the statistical approach of the RSM model to simultaneously determine the optimum condition for MOR. From our knowledge, there is no previous optimization work on bio-inspired Pt NPs synthesized from agricultural waste *S. officinarum L.* bagasse extract in electro-oxidation fuel cell studies using the RSM technique, making our study innovative and superior. Further, this study aimed to investigate the intrinsic kinetic activity of bio-inspired Pt NPs in MOR under the influence of Pt NP concentration, methanol concentration, and temperature conditions, as well as the physicochemical characteristics. Finally, the bio-inspired Pt NPs will be evaluated as the anode electrode in the passive single-cell direct methanol fuel cell.

2. EXPERIMENTAL

2.1 One-step green synthesis of bio-inspired Pt NPs catalyst

In a typical experiment of the chemical reduction method, the *S. officinarum*, L. bagasse extracts were added dropwise to a varied concentration solution of 0.5, 1.0, 1.5, and 1.75 mM $H_2PtCl_6.6H_2O$ in a conical flask and heated up to 100º C following our previous studies,

denoted as Bio-$Pt_{0.5}$, Bio-$Pt_{1.0}$, Bio-$Pt_{1.5}$, and Bio-$Pt_{1.75}$, respectively (Ishak et al., 2020), (Nurul Atiqah Izzati Md Ishak, S.K. Kamarudin, Sharifah Najiha Timmiati, Nabila Karim, 2021). After the reaction was completed by observing the changes to a black solution, then the colloidal suspension was sonicated, and afterward, it was washed using deionized water by being repeatedly centrifuged. Finally, the purified pellet was dried at 110 ºC for 6 hours.

2.2 Electrochemical analysis

The electrochemical measurements of bio-inspired Pt NPs for MOR performance were conducted using an Autolab PGSTAT204 (Netherlands) instrument with the features of a three-electrode system consisting of a glassy carbon electrode (GCE), Ag/AgCl sat. KCl as the reference electrode, and a Pt rod as the counter electrode. 2.5 µL of bio-inspired Pt NPs dispersion from a mixed ink catalyst of deionized water, 2-propanol, and 5% Nafion® solution was dropped onto a GCE surface and let dry. MOR tests were conducted in 0.5 M H_2SO_4 with or without 1 M CH_3OH in a potential window of -0.25 and 1.0 V (vs. Ag/AgCl). The same procedure was also compared on a commercial Pt black (HiSPEC 1000, Alfa Aesar, USA).

2.3 Design of Experiment

The experimental design involves a screening one-factor-at-a-time (OFAT) experiment to identify key factors and estimate required factor values before optimizing using the RSM method. Design Expert 10.0.3 software (Stat-Ease Inc., Minneapolis, USA) was used to produce a platform to perform parameter optimization via RSM. In this study, the Central Composite Design (CCD) design was selected to determine the optimal factor values for the MOR using bio-inspired Pt NPs as an electrocatalyst. The variables used were the bio-Pt NPs concentration (X_1), electrocatalyst loading (X_2), and CH_3OH concentration (X_3). The response measured in this study is the current density (mA/mg_{Pt}) of MOR. Factor codes and

experimental levels are presented in Table 1. Based on CCD analysis, the experimental arrangement uses a matrix design. According to CCD, the total experiment number for three parameters was determined to be 20 using the equation $2^k + 2k + 6$, where k is the number of independent parameters. The experimental data were adjusted with a polynomial regression model, expressed by Eq. (1):

$$y = \beta_0 + \sum_{i=1}^{3} \beta_i X_I + \sum_{i=1}^{3} \beta_{ii} X_i^2 + \sum_{ij>j}^{a}. \sum_{j}^{3} \beta_{ii} X_i X_j \quad (1)$$

Where, y = response variable (current density); X_i and X_j = are the independent parameters i.e., bio-inspired Pt NPs concentration, electrocatalyst loading, and CH_3OH concentration; β_0, β_i, β_{ii}, β_{ij} = fixed term i.e., is a constant coefficient, (β_0 is a constant, β_i is a coefficient for linear terms, β_{ii} is a coefficient for quadratic terms; β_{ij} is a coefficient for second-order interaction terms). The predicted model is evaluated by analyzing the values of regression coefficients, ANOVA, F-value, and P-value. The appropriate quality of the polynomial equation model is determined by the regression coefficient, R^2 near 1, and insignificant lack-of-fit. Validation experiments are then conducted to confirm the predictive value derived from the model using the optimal values of these three factors.

Table 1. Experimental ranges and levels of the independent parameters studied in CCD.

Independent parameters	**Symbol**		**Range and level**		
	Uncoded	Coded	-1	0	+1
Bio-Pt NPs concentration (mM)	X_1	x_1	0.5	1.0	1.5
Electrocatalyst loading (g)	X_2	x_2	1.5	2.0	2.5
CH_3OH concentration (M)	X_3	x_3	1	1.5	2.0

2.4 Membrane electrode assembly (MEA) preparation and passive single cell DMFC performance

The selected bio-Pt NPs were tested as anode porous layers in membrane electrode assembly (MEA). MEA comprises a membrane and two electrodes, with a Nafion 117 proton exchange

membrane sandwiching between the anode and cathode electrocatalysts. Prior to MEA fabrication, the Nafion 117 membrane (DuPont Inc., USA) was protonated as applied in Hasran et al. (Hasran et al., 2013) by sequent immersed in a beaker of deionized water and boiling solution of 3 vol.% H_2O_2, both for 1h at 80 ºC. Then, the Nafion 117 membrane was immersed in deionized water for 20 minutes to rinse before immersed in 1 M H_2SO_4 at 80ºC for 1 h. Finally, the membrane was placed in a beaker of boiling deionized water to remove any impurities and produce a clear transparent membrane. The protonated membrane was then stored in deionized water until it was ready to use.

The next process is to fabricate a microporous layer (MPL). An Electrochem, Inc. carbon cloth (CC-060) was used as the anode and cathode backing layer and was treated by immersing in 5 wt % of polytetrafluoroethylene (PTFE) solution and dried at 380 ºC for 30 minutes. The MPL is composed of Vulcan XC-72 carbon powder mixed with deionized water, isopropanol, and Nafion dipersion D520 (DuPont), with each stage being sonicated for 10 to 15 minutes to create a carbon slurry. The carbon slurry was then cast on the hydrophobic carbon cloth and dried in an oven at 100 ºC for 1 h to form a gas diffusion layer (GDL). The backing layer is covered with a GDL of carbon, with a loading of 2 mg cm^{-2}. Then, 8 mg cm^{-2} loading of the bio-Pt NPs electrocatalyst was mixed with 1000 µL deionized water, 1500 µL isopropanol and Nafion dispersion (34 mg) was uniformly brushed on the GDL to form the anode electrode. Meanwhile, 8 mg cm^{-2} loading of the Pt black commercial (HiSPEC 1000, Alfa Aesar, USA) serves as cathode electrode is prepared similarly. Then, the anode and cathode catalyst layer were dried at 110 ºC for 1 h. For comparison, commercial Pt black with same loading and method preparation were also evaluated. Eventually, the MEA was fabricated in-house by hot pressing at 135 ºC and 30 bars for 180 s. A schematic diagram of the experimental setup is shown in Fig. 1.

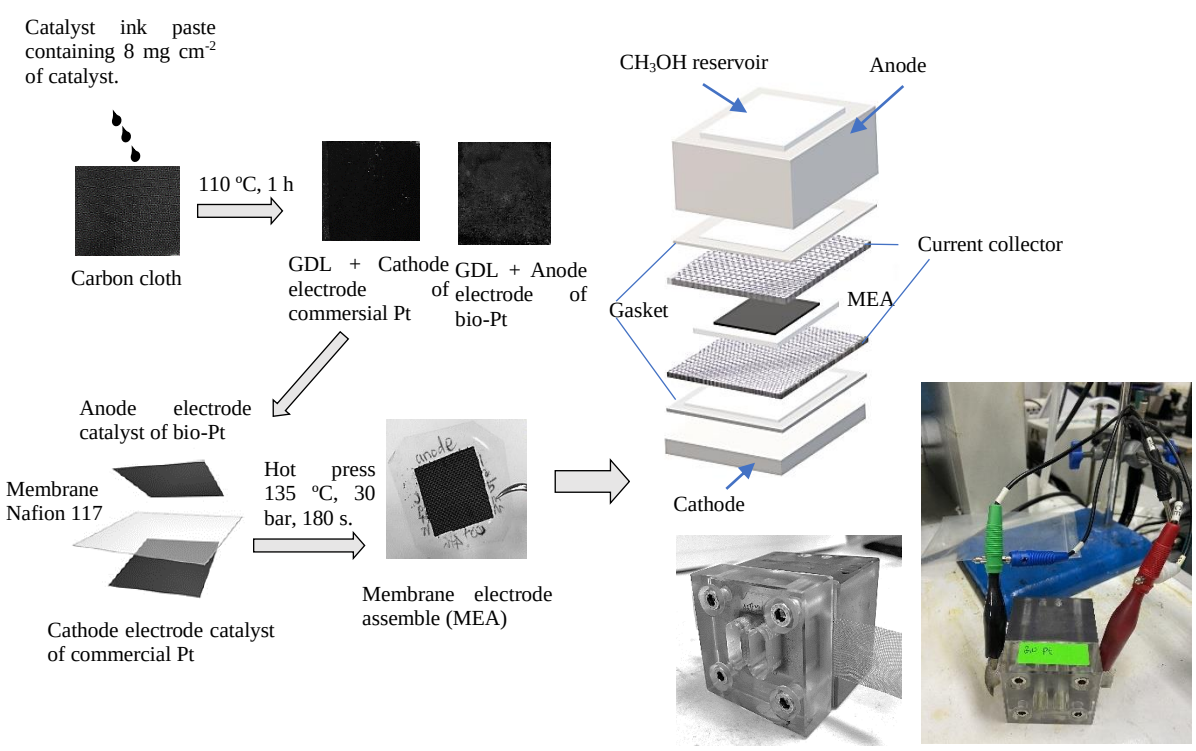

Fig. 1. Schematic process of MEA fabrication and structure of passive DMFC single cell components.

2.5 Operation of Passive Single cell DMFC performance

The bio-Pt NPs was further envisaged as anode electrode in a geometric area of 4 cm^2 passive single cell DMFC with a built-in 10 ml methanol solution container. The MEA was mounted into the single cell and operated passively with 2 M CH_3OH injected into the anodic compartment. A potentiostat (Zive, WonATech Co., Ltd, Korea) was used to measure the voltage, current density, and power density of the cell at room temperature and atmospheric. The working electrode and working sense were connected, and the reference electrode was connected to the counter electrode and clipped onto the end terminal current collector of the single cell DMFC, as shown in the Fig. 1. The voltage response and current values of the cell were recorded by Zive Zman software, allowing for the collection of I-V polarization data.

3. RESULTS AND DISCUSSION

3.1 Physicochemical properties of synthesized bio-inspired Pt NPs

Herein, we demonstrate a green chemical reduction through the biosynthesis route by using plant extract as a reducing agent toward fabricating Pt NPs with compositions that are tunable. The crystallographic characteristics of all bio-Pt NPs were first examined using XRD analysis (Fig. 2). The resulting bio-Pt NPs were denoted as Bio-$Pt_{0.5}$, Bio-$Pt_{1.0}$, Bio-$Pt_{1.5}$, and Bio-$Pt_{1.75}$. The five distinct peaks of the face-centered cubic (*fcc*) structure of platinum were observed in all samples and corresponded to the (111), (200), (220), (311), and (222) planes. All the peaks are located in the standard diffraction peaks of Pt (JCPS No. 04-0802) and represent the typical profile of polycrystalline Pt (Ocampo-Restrepo et al., 2017).

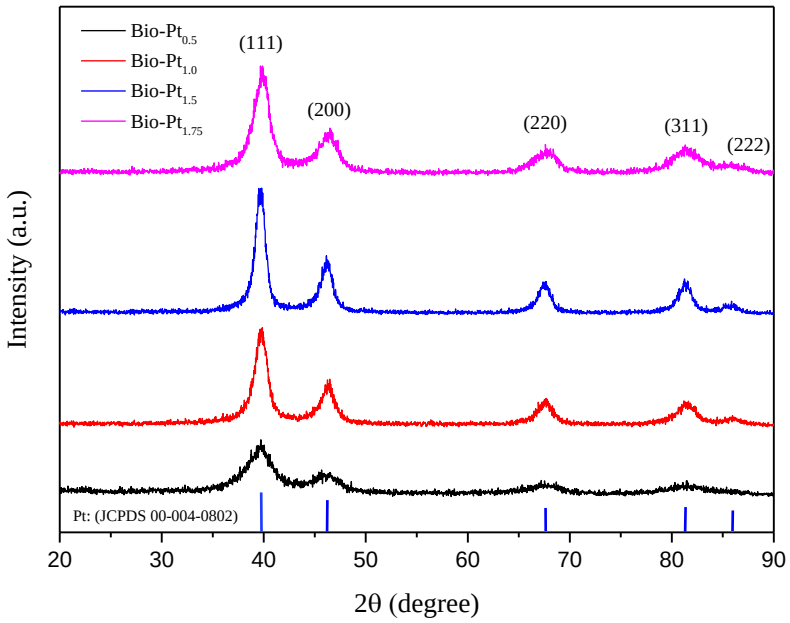

Fig. 2. XRD patern for bio-inspired Pt NPs with varied molar concentrations of 0.5, 1.0, 1.5 and 1.5 mM.

The size, shapes, and distributions of all bio-inspired Pt NPs were then examined by TEM at various magnifications to ascertain the impact of different Pt NP concentrations. Figs. 3a - 3d represent the TEM images of bio-inspired Pt NPs with different concentrations of 0.5, 1.0, 1.5, and 1.75 mM, respectively. From the overall images in Figs. 3a – 3d, a uniform distribution and nanosize of all bio-Pt NPs were successfully achieved through the biosynthesis route through plant mediated as reducing agents. Interestingly, this plant mediated synthesis has a significant impact on the shape and size control of Pt NPs. The

effect of Pt NP concentration on morphological changes was seen as anisotropic structures began to emerge as concentration increased. Based on Figs. 3a and 3b, the resulting Bio-$Pt_{0.5}$ and Bio-$Pt_{1.0}$ have a spherical shape.

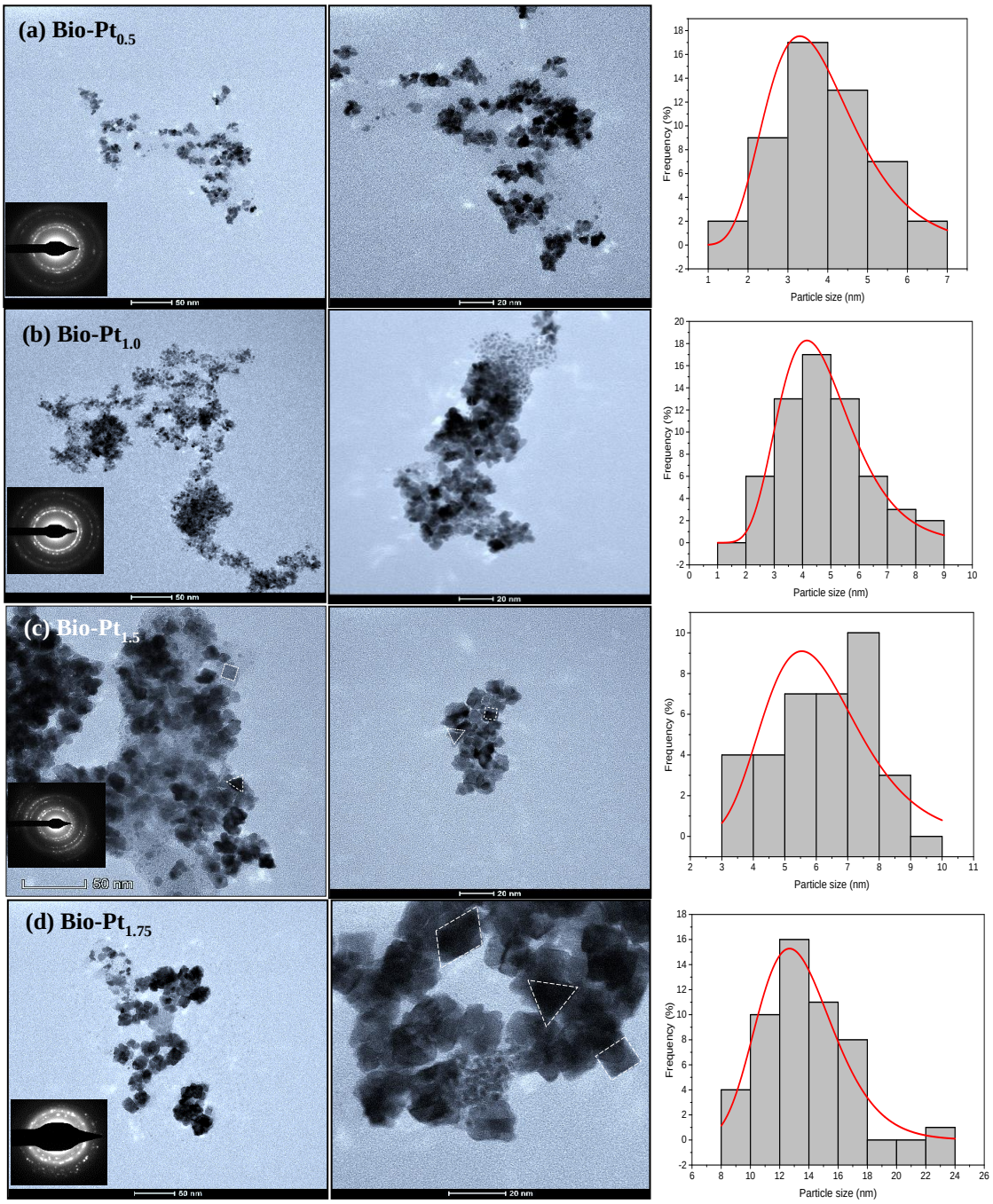

Fig. 3. TEM image, particle size distribution histogram, and SAED pattern of concentration-tunable bio-inspired Pt NPs of (a) Bio-$Pt_{0.5}$, (b) Bio-$Pt_{1.0}$, (c) Bio-$Pt_{1.5}$, and (d) Bio-$Pt_{1.75}$.

As the concentration increases to 1.5 and 1.75 mM, the Bio-$Pt_{1.5}$ and Bio-$Pt_{1.75}$ start to emerge as anisotropic structures comprising cubic, triangle, and rhombus shapes despite

mostly displaying spherical shapes. Besides, the mean of particle sizes is also increased as the concentration is elevated from 0.5 to 1.75 mM. The mean particle sizes of Bio-$Pt_{0.5}$, Bio-$Pt_{1.0}$, Bio-$Pt_{1.5}$, and Bio-$Pt_{1.75}$ are 3.85 ± 1.15, 4.75 ± 1.4, 6.15 ± 1.53, 13. 47 ± 2.76 nm, respectively, as portrayed in the histogram bar shown in the inset of Fig. 3. Based on the micrograph, the spherical shape is found to have a smaller size compared to the anisotropic structure. Another inset of Fig. 3 shows the Selected Area Electron Diffraction (SAED) with four bright rings pattern that indicate the degree of crystallinity, suggesting the polycrystallinity of the Pt NPs and resembling the index planes of (111), (200), (220), and (311) reflections of face-centered cubic phase that are congruent to XRD analysis.

3.2 Electrochemical evaluation and kinetic reaction assessment on methanol oxidation reaction (MOR)

3.2.1 Electrochemical active surface area (ECSA)

To verify the effectiveness of this plant-mediated biosynthesis route, the electrocatalytic activity of these bio-inspired Pt NPs was demonstrated in the MOR. This path was believed to have exposed the surface area of the bio-inspired Pt NPs with many catalytically active sites, offering a promising avenue for making electrocatalysts. To measure the attainable active sites of the bio-inspired Pt NPs, cyclic voltammetry (CV) measurement was performed in N_2-saturated 0.5 M H_2SO_4 solution (Fig. 4a) to determine the electrochemical active surface area (ECSA) value. The calculated ECSA value by integrating the H_2 desorption peak for Bio-$Pt_{1.5}$ delivers the highest ECSA of 93.41 $m^2\ g^{-1}$, exceeding that for commercial Pt black (27.49 $m^2\ g^{-1}$), Bio-$Pt_{0.5}$ (18.63 $m^2\ g^{-1}$), Bio-$Pt_{1.0}$ (77.16 $m^2\ g^{-1}$), and Bio-$Pt_{1.75}$ (16.05 $m^2\ g^{-1}$).

3.2.2 Effect of bio-inspired Pt NPs concentration on MOR

The high ECSA value demonstrated by the bio-inspired Pt NPs could significantly enhance the MOR and accelerated the faster electron transfer during the electrochemical reaction. Therefore, Bio-$Pt_{1.5}$ exhibits the highest peak catalytic current density toward MOR, reaching

581.50 mA/mg_{Pt}, by a factor of 3.67 than that of commercial Pt black (158.12 mA/mg_{Pt}) (Fig. 4b). The effect of Pt NPs concentration, [Pt NPs] varied from 0.5 to 1.75 mM (Bio-$Pt_{0.5}$, Bio-$Pt_{1.0}$, Bio-$Pt_{1.5}$, and Bio-$Pt_{1.75}$) was observed that with increasing the [Pt NPs], the methanol oxidation peak referring to the current density was found to increase from 0.5 to 1.5 mM i.e., from 46.35 mA/cm^2 (230.36 mA/mg_{Pt}) to 117.00 mA/cm^2 (581.50 mA/mg_{Pt}). However, the current density decreased to 16.05 mA/cm^2 (98.89 mA/mg_{Pt}) when the [Pt NPs] was increased to 1.75 mM, as presented in Fig. 4b - c. This is due to the increasing and saturated total concentration of Pt on the active site of the electrocatalyst, preventing the adsorption of methanol molecules on it. This parameter confirms that the concentration of bio-inspired Pt NPs has a significant effect on the current density of MOR.

Kinetic studies in the MOR for bio-inspired Pt NPs can be examined via Tafel plot analysis, charge transfer coefficient (α), and exchange current density, j_0. The linear regions of Tafel plots in Fig. 4c are fitted to the Tafel equation, yielding Tafel slopes of 199 (α = 0.30), 191 (α = 0.31), 170 (α = 0.35), 241 (α = 0.25) and 233 (α = 0.25) mV/dec for Bio-$Pt_{0.5}$, Bio-$Pt_{1.0}$, Bio-$Pt_{1.5}$, Bio-$Pt_{1.75}$ and commercial Pt black, respectively. Tafel slopes with lower values suggest a higher kinetic rate of the MOR process that results in faster hydrogenation rates and lower overpotentials, representing the first rate-determining step of CO_{ad} migration from the Pt active site, as demonstrated by Bio-$Pt_{1.5}$. The kinetic parameters for all electrocatalysts presented in Table 2 are derived from the Tafel equation:

$$\eta = \alpha + b \log j \quad (2)$$

where η (V) is the overpotential, α (V) is the intercept, b (mV/dec) is the Tafel slope, and j (mA cm^{-2}) is the current density.

The constant of ‘α’ and ‘b’ can be expressed as:

$$\alpha = (2.303RT)/(\alpha F) \log j_0 \quad (3)$$

$$b = (2.303RT)/(\alpha F) \quad (4)$$

where R is the universal gas constant (8.314 kJ mol^{-1} K^{-1}), T is the temperature in K, α is the charge-transfer coefficient, and *F* is the Faraday constant (96,485 C mol^{-1}). The j_0 can be calculated by applying $j_0 = 10^{-\alpha/b}$ according to the relationship between η and log *j*. The calculated values of j_0 are: 3.58, 28.5, 6.25, 15.67 and 2.13 μA cm^{-2} for Bio-$Pt_{0.5}$, Bio-$Pt_{1.0}$, Bio-$Pt_{1.5}$, Bio-$Pt_{1.75}$, and commercial Pt black, respectively.

Table 2. Tafel slope (b), charge transfer coefficient (α), and exchange current density (j_0) for bio-Pt NPs catalysts in 0.5 M H_2SO_4 + 1.0 M CH_3OH.

Electrocatalysts	**Tafel slope (mV/dec)**	**Charge transfer coefficient, (α)**	**Exchange current density, j_0 (mA cm^{-2})**
Bio-$Pt_{0.5}$	199	0.30	0.0358
Bio-$Pt_{1.0}$	191	0.31	0.2858
Bio-$Pt_{1.5}$	171	0.35	0.0625
Bio-$Pt_{1.75}$	241	0.25	0.1567
Commercial Pt black	233	0.25	0.0213

To correlate the obtained CV in MOR performance, there is a relationship between the synthetic parameter on the morphological structure and the percentage of Pt species present with the current density yield. XPS characterized the chemical states and composition of bio-Pt NPs. Fig. 5 shows the relationship between the XPS spectra of Pt elements, and the morphological structure of Bio-$Pt_{0.5}$, Bio-$Pt_{1.0}$, Bio-$Pt_{1.5}$, and Bio-$Pt_{1.75}$ as influenced by Pt concentration. The integrated peak area of XPS suitability, the calculated species density ratio, and the percentages of Pt (0), Pt (II), and Pt (IV) obtained and correlated with the current density produced are shown in Table 3. Three pairs of peaks can be fitted to the Pt 4f spectrum of the bio-Pt NPs to determine the different oxidation states of Pt. The $4f_{7/2}$ signal is observed in all spectra of the bio-inspired Pt NPs at around 71.4 - 74.8 eV, and this signal represents the Pt (0). The peaks corresponding to 74.0–75.0 eV and 72.4–74.9 eV refer to Pt^{4+} and Pt^{2+}, respectively, which are derived from PtO_2 and/or Pt $(OH)_4$ (Eris et al., 2018). The percentage of integration of the bio-inspired electrocatalyst peak areas of Bio-$Pt_{1.0}$ and Bio-

$Pt_{1.5}$, has the highest Pt (0) species, which is the Pt ion of metal nanoparticles that have been successfully reduced to ~ 73 %.

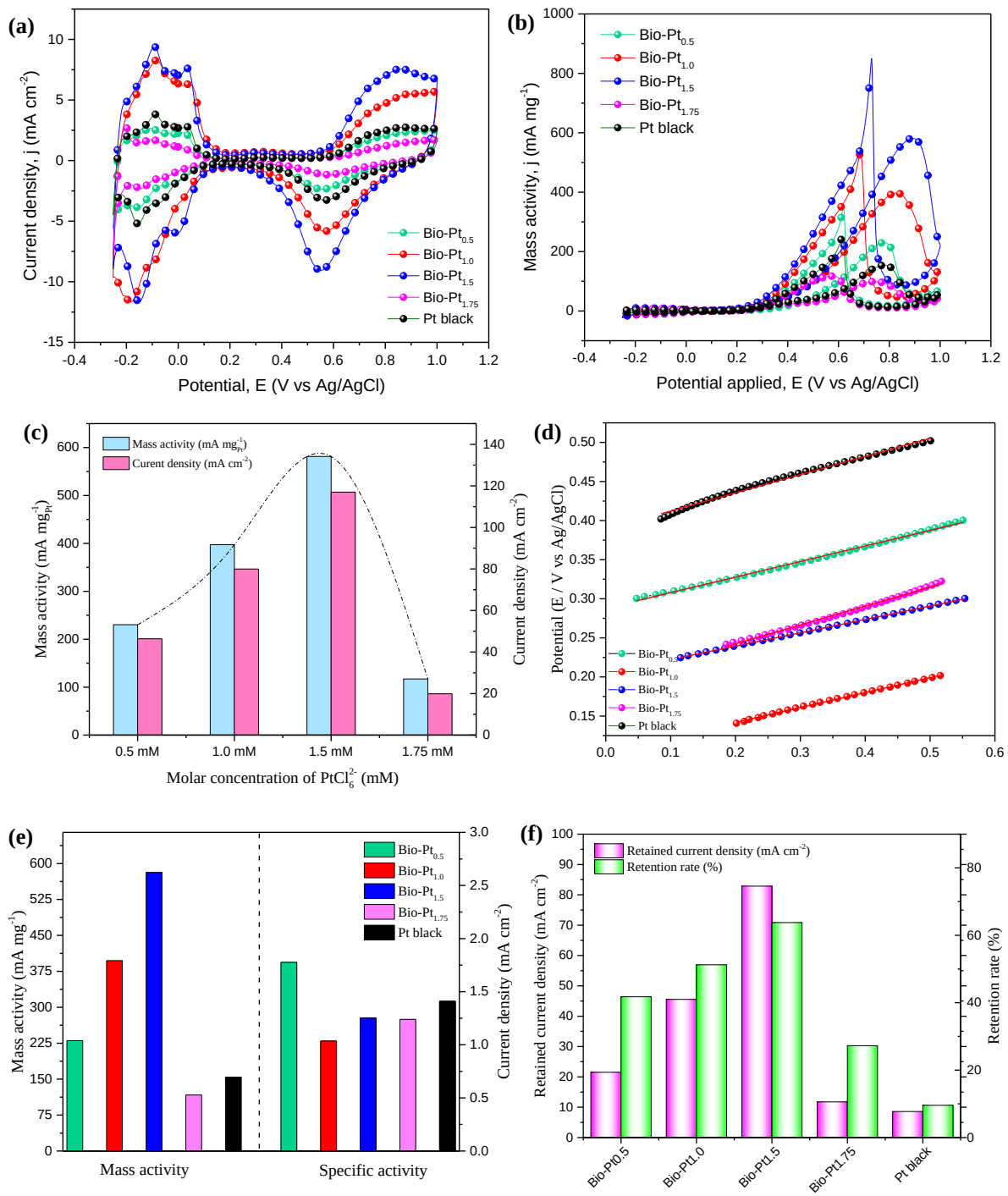

Fig. 4. CV voltammogram of bio-inspired Pt at different concentrations from the range of 0.5 to 1.75 mM (a) H_2 adsorption/desorption in 0.5 M H_2SO_4, (b) methanol oxidation in 0.5 M H_2SO_4 + 1.0 M CH_3OH, (c) current density trend, (d) Tafel plot, (e) comparison in specific area and mass activity of MOR at different bio-Pt NPs concentration, and (f) the retained current density (mA cm^{-2}) and retention rate of all electrodes from chronoamperometry test.

Increasing the percentage of metallic Pt (0) area, promotes an increase in the large number of active sites, and is supported by the high ECSA value as shown in Table 3 and accompanied by a uniform and nanosized nanoparticle distribution, resulting in the highest current density exhibited by Bio-$Pt_{1.5}$. The diameter size was found to increase with the increasing concentration of Pt NPs. The average diameter size of the bio-inspired electrocatalyst Bio-$Pt_{0.5}$ was 3.85 nm, while Bio-$Pt_{1.0}$ was 4.75 nm. A sharp four-angle image such as rhombus morphological geometry for Bio-$Pt_{1.75}$ has a length of 22.86 nm and a rectangle of 17.19 nm, while a triangle has a length of 15.83 nm compared to Pt NP of concentration 1.5 mM, Bio-$Pt_{1.5}$, which has a triangle length of 7.89 nm and a rectangle with a size of 7.87 nm. By increasing Bio-$Pt_{1.75}$, particles become larger, and the calculated species density of Pt (0) decreases, causing the ECSA value to decrease, which explains the lower performance of Bio-$Pt_{1.75}$ in MOR activities. As a result of this finding, it is likely that the higher valence state of Pt is related to the high mass/specific activity (Hui et al., 2022).

Table 3. Integral percentage of peak area to calculate Pt species formed and particle size diameter with current density (mA/mg_{Pt}).

Electrocatalyst bio-Pt NPs	**Pt (0) 71.5 eV**	**Pt (II) 72.4 eV**	**Pt (IV) 75.0 eV**	**Diameter size (nm)**	**Mass activity, j (mA/mg_{Pt})**	**ECSA ($m^2 g^{-1}$)**
Bio-$Pt_{0.5}$	51.63 %	32.76 %	15.59 %	3.85	230.36	18.63
Bio-$Pt_{1.0}$	72.97 %	27.02 %	-	4.75	397.35	77.16
Bio-$Pt_{1.5}$	73.32 %	26.70 %	-	15.83	581.50	93.41
Bio-$Pt_{1.75}$	47.08 %	22.70 %	30.20 %	22.86	98.89	16.05

To track the CO-tolerance against carbonaceous species, the I_f/I_b ratio were extracted from the peak current density of the MOR CV curve of the forward scan (I_f) to backward (I_b) scan. By analyzing the I_f/I_b peak current density ratio, it can determine the extent to which carbonaceous species are affecting the catalytic activity (Cheng et al., 2022). The determined value of I_f/I_b for Bio-$Pt_{0.5}$, Bio-$Pt_{1.0}$, Bio-$Pt_{1.5}$, and Bio-$Pt_{1.75}$ were 0.66, 0.74, 0.68, and 0.85. The low I_f/I_b ratio may be explained by a lower Pt surface covered by oxygenated species, resulting in a greater I_b in the backward scan (Md Ishak et al., 2023). This suggests that the

oxygenated species on the Pt surface are not as stable or abundant during the backward scan, leading to a higher current in the opposite direction (Toghan et al., 2021). Additionally, it is possible that other factors such as electrode morphology or reaction kinetics could also contribute to this observed difference in I_b.

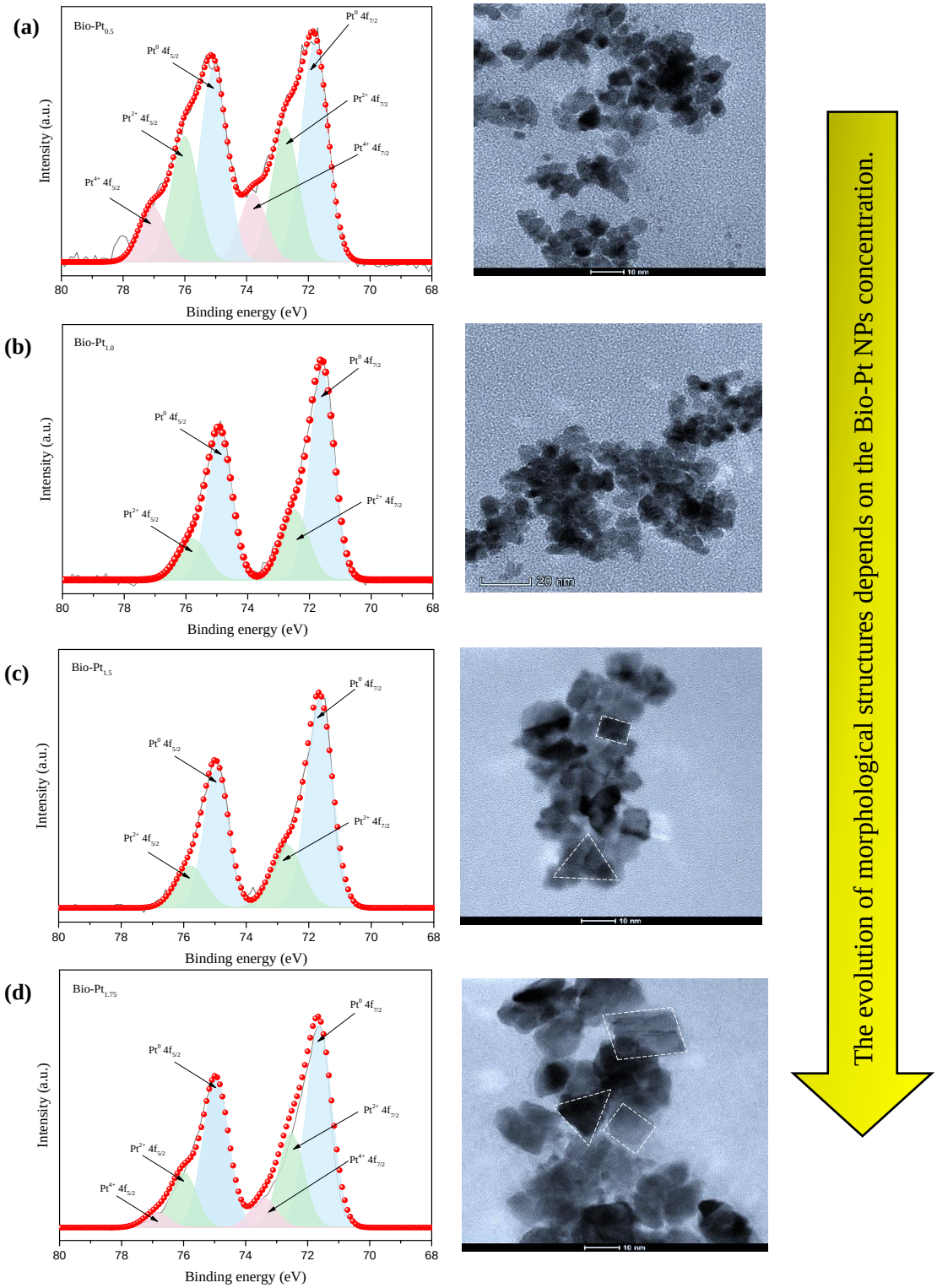

Fig. 5. XPS spectra of bio-inspired Pt element species density ratio and morphological structure correlation on TEM image with diverse influence of bio-Pt concentration of (a) 0.5 mM (Bio-$Pt_{0.5}$), (b) 1.0 mM (Bio-$Pt_{1.0}$), (c) 1.5 mM (Bio-$Pt_{1.5}$), and (d) 1.75 mM (Bio-$Pt_{1.75}$).

To gain a better understanding of the performance of methanol electrooxidation, the chronoamperometry (CA) test is used to investigate the stability of bio-inspired Pt NPs. During the test, the oxidation reaction of methanol molecules is continuously processed on the electrode, resulting in a rapid drop in current at the initial stage because the methanol dehydrogenation mechanism produces intermediate carbonaceous species that occupy the active site of the catalyst and impact the catalyst performance drop. As the reaction rate lowers, the residue methanol concentration reaches constancy; on the one hand, the CO adsorption and oxidation achieve an equilibrium state, and the CA curve remains stable (Ding et al., 2021). The reserved value and retention rate can measure explicitly the stability of the catalysts, as illustrated in Fig. 4f. Apparently, Bio-$Pt_{1.5}$ showed the highest retention rate of 70.83% and the lowest retention rate was Pt black of about 22.11%, and superior to Bio-$Pt_{1.0}$ (56.94%) > Bio-$Pt_{0.5}$ (46.38%) > Bio-Pt1.75 (30.26%). Hence, conceivably, speculate the biosynthesis method-plant mediated improvises the electrocatalytic properties of bio-inspired Pt nanostructures.

3.2.3 Effect of scan rate on MOR and reaction kinetics

Other parameters influencing methanol oxidation activity can be measured by scan rate variability techniques. Fig. 6a and 6b illustrate the bio-Pt NPs and commercial Pt black voltammograms subjected to different scan rates from 10 to 100 mV s^{-1} in 0.5 M H_2SO_4 + 1.0 M CH_3OH. To study the kinetics of methanol oxidation by bio-Pt NPs and commercial Pt black electrocatalysts, the relationship between anodic peak current (j) and peak potential (E_p) as a function of the different scan rates (v) was studied and shown in Fig. 6c. The observation shows that increasing the scan rate causes the oxidation peak of E_p MOR to

increases and result in a more positive direction. Fig. 6c shows that the anodic peak current of the E_p MOR increases linearly with the square root of the scan rate, ($\nu^{1/2}$) which is a sign that the methanol oxidation reaction by bio-Pt NPs is a diffusion-controlled process (Shafaei Douk et al., 2018b). This linear relationship proves that mass transport controls the methanol oxidation reaction (Ojani et al., 2015), (Shafaei Douk et al., 2018a). Furthermore, the anodic peak potential is also increased linearly with ln (ν) as shown in Fig. 6d, indicating that methanol oxidation is an irreversible electrode process (Li et al., 2011). According to the plotted graph from Fig. 6c, a linear relationship between peak current density, *j vs* the square root of the scan rate, ($\nu^{1/2}$), an Eq. (5) is obtained:

$$I_f \text{ (mA cm}^{-2}) = 9.04359\ \nu^{1/2}\text{ (mV/s)} + 6.74123,\ R^2 = 0.8088 \quad (5)$$

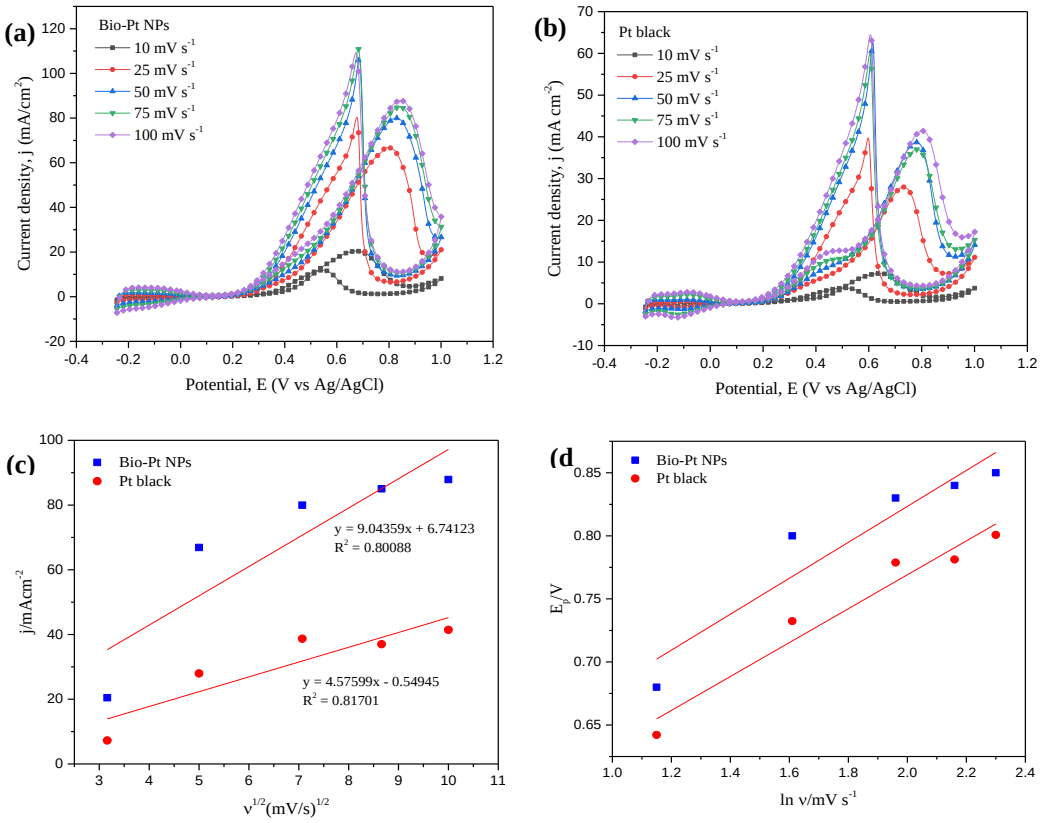

Fig. 6. MOR voltammograms at different scan rates of 10 – 100 mV s^{-1} for (a) bio-Pt NPs and (b) commercial Pt black and (c) plot of anodic peak current density, *j* against the square root of scan rate, $\nu^{1/2}$ and (d) peak potential, E_p as a function of ln scan rate, ν for MOR of bio-Pt NPs and commercial Pt black.

The higher slope given by bio-inspired Pt NPs shown in Fig. 6c and 6d indicates superior MOR kinetics in the rate-determining step (Huang et al., 2017), (W. Chen et al., 2020). It can be concluded that the bio-Pt NPs electrode has higher electrocatalytic activity in MOR than the commercial Pt black electrode. Another parameter that can be studied from the evaluation of different scan rates is the methanol diffusion coefficient. Methanol diffusion coefficients were calculated using the Randles-Sevcik equation according to Li et al. (2011):

$$I_p = 0.4463nFAC(\frac{nF\nu D}{RT})^{0.5} \quad (6)$$

Where, I_p, n, C and D represent the peak current density (mA cm^{-2}), the number of electrons involved in the reaction (n = 6), the methanol concentration (mol cm^{-3}) and the diffusion coefficient (cm^2 s^{-1}), respectively. F is the Faraday constant (96,485 C mol^{-1}), A is the electrode surface area, R is the universal gas constant (8.314 J/K.mol) and T is the absolute temperature (298 K). The methanol diffusion coefficient, D calculated for the bio-Pt NPs is 1.96 x 10^{-6} cm^2 s^{-1} which is higher than the commercial Pt black, which is 3.82 x 10^{-7} cm^2 s^{-1}. The D value of the bio-Pt NPs electrocatalyst approaches the D value of 2,369 x 10^{-9} m^2 s^{-1} described by Derlacki et al. (1985) for 1.0 M CH_3OH in aqueous solution at 298 K.

The reaction kinetics on the electrode surface are also studied because they are essential for a better understanding of the heterogeneous electron transfer process. Based on the relationship between peak current and peak potential of the complete, irreversible electrode reaction, a 'k_s' rate constant for methanol electrooxidation on a fuel cell electrocatalyst can be calculated as recommended by Ma et al. (2013):

$$I_f = 0.227nFACks\ exp\ (\frac{\alpha F}{RT}(E_f - E^0)) \quad (7)$$

Where n, A, and C are the total number of electrons transferred in the overall reaction (in this case, it is 6), the surface area of the electrode (0.071 cm^2), and the bulk concentration of the reactant (in this case, 0.001 mol cm^{-3}). Other parameters have common meanings. Based on Eq. (6) and Eq. (4), it is obtained (Ma et al., 2013):

$$k_s = \frac{If}{9.33}\, exp\, \frac{2.303}{b}\, (E^0 - E_f) \quad (8)$$

Hence, Eq. (8) is used to evaluate the rate constant, k_s. For convenience, the values of E^0 were taken as 0.8 and 0.7 V for reference purposes in polarization measurements for bio-Pt NPs and commercial Pt black, respectively. The value of the rate constant, k_s for the bio-Pt NP was 0.0421 cm s^{-1} mg^{-1} Pt and was found to be 2.48 times higher than the k_s of the commercial Pt black, which was 0.017 cm s^{-1} mg^{-1}Pt.

3.2.4 Effect of methanol concentration on MOR and reaction order

Further electrokinetic studies concerned the influence of CH_3OH concentrations in the range of 0.3 to 2.0 M in 0.5 M H_2SO_4 at a scan rate of 50 mV s^{-1} was evaluated in Fig. 7a. The order of the bio-Pt NPs electrocatalyst reaction for the MOR was quantified according to the following equation by plotting the logarithm of the anodic current density against the logarithm of the methanol concentration (Amin et al., 2012):

$$\text{Rate} = I_p = kC^n \quad (10)$$

$$\log j = \log k + n \log C \quad (11)$$

Where j is the forward anodic sweep current density, k is the reaction rate constant, n is the reaction order, and C is [CH_3OH].

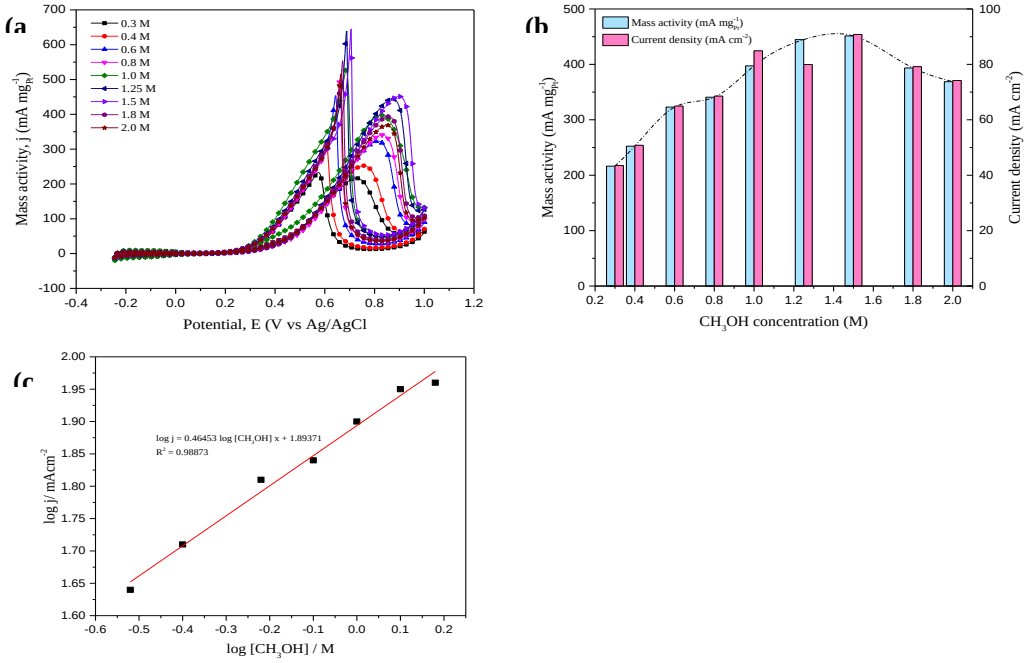

Fig. 7. (a) MOR voltammogram of bio-Pt NPs at CH_3OH concentration range from 0.3 – 2.0 M, (b) performance comparison graph and, (c) logarithm plot of anodic peak current (log *j*) *vs* logarithm of methanol concentration (log *C*).

As illustrated in Fig. 7a, a MOR voltammogram with CH_3OH concentrations varying from 0.3 M to 2.0 M resulted in an increase in the current density and anodic peak potential (Ekrami-Kakhki et al., 2019). Higher methanol concentrations promote a linear increase in MOR current density. Studies on the influence of CH_3OH concentration on bio-Pt NPs activity showed that 1.5 M CH_3OH was the optimum concentration by recording a current density of 451.40 mA mg^{-1}_{Pt}. However, as can be seen in Fig. 7b, when the methanol concentration increases to 1.8 M, the pattern begins to decline. This condition indicates that the active site has been saturated, and because of poisoning by the carbonate intermediate species adsorbed on the surface of the electrocatalyst (Ojani et al., 2015). Nevertheless, plots for the logarithm of the peak oxidation current density *vs*. the logarithm of the methanol concentration show a linear relationship (see Fig. 7c). From the slope of the logarithmic plot, the following Eq. (11) is obtained, the order value of the reaction, α is around 0.46.

$$\text{Log } j = 0.46453 \log [CH3OH] \text{ x} + 1.89371, R^2 = 0.98873 \quad (12)$$

3.2.5 Effect of temperature on MOR

Fig. 8a and 8b illustrate the effect of temperature at 25-60 ºC on the oxidation rate of methanol in 0.5 M H_2SO_4 + 1.0 M CH_3OH using bio-Pt NPs and commercial Pt black at 5 mV s^{-1}. The MOR current density increases with temperature and the shape of the polarization curve does not change. This indicates that the MOR mechanism remains constant, but the reaction rate changes. Arrhenius plots of methanol oxidation in acidic medium derived from Fig. 8a and 8b were shown in Fig. 8c and 8d, respectively, and were calculated using the following equations (Jing et al., 2013):

$$i = Ae^{-Ea/RT} \quad (13)$$

As described in the Arrhenius Equation, the current in the region of low overpotential is related to temperature in logarithmic form and can be determined by the following equation (Velázquez-Palenzuela et al., 2011):

$$\log i = \log A - \frac{Ea}{2.3R}\left(\frac{1}{T}\right) \quad (14)$$

where A is a frequency constant; T = temperature, K; R = universal gas constant, 8.314 J/K.mol; and E_a = activation energy, kJ.mol^{-1}. By performing the linear equation ln i against T^{-1}, E_a can be determined from the plot gradient values for the bio-Pt NPs and the commercial Pt black.

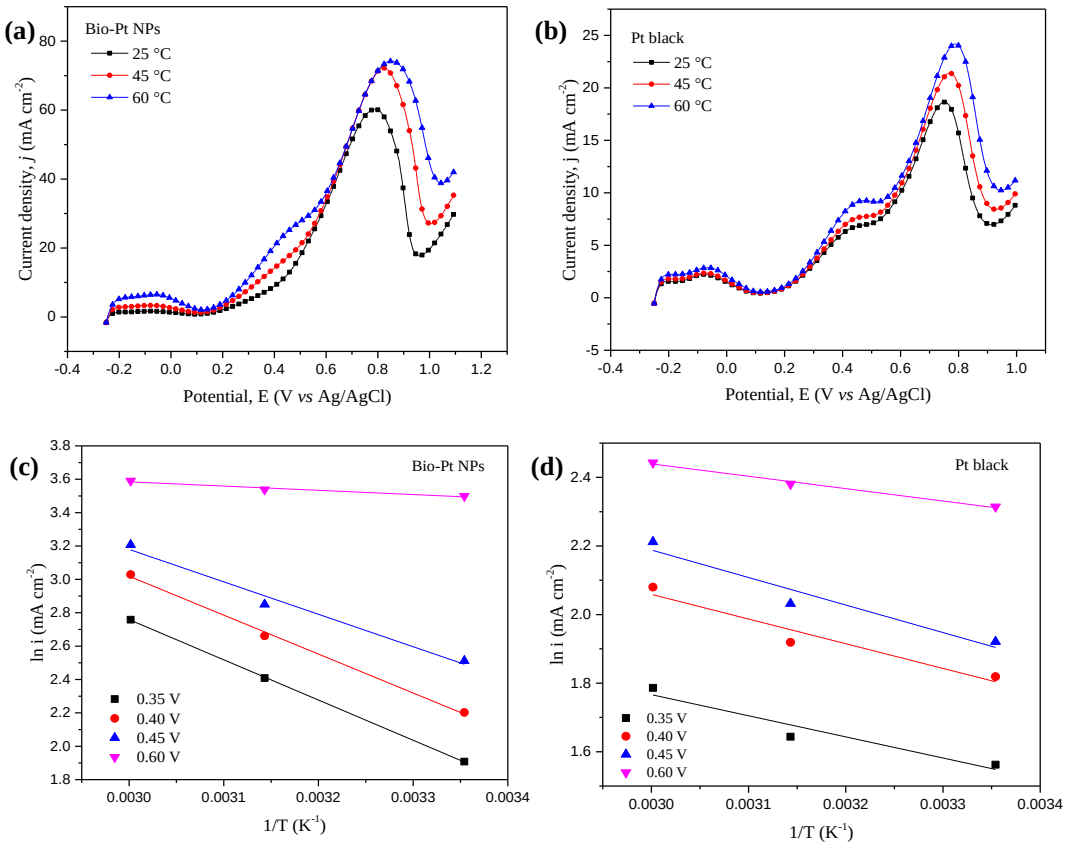

Fig. 8. Polarization curves of methanol oxidation at different temperatures of 25, 45, and 60 ºC at a scan rate of 5 mV s^{-1} of (a) bio-Pt NPs and (b) commercial Pt black; and Arrhenius plot of ln i (mA cm^{-2}) *vs*. temperature (K^{-1}) of methanol oxidation measured at different potentials 0.35 – 0.60 V for (c) bio-Pt NPs and, (d) commercial Pt black.

Each plot in Fig. 8a and 8b shows good linearity. The value of activation energy, E_a calculated from the slope of this Arrhenius plot for bio-Pt NPs is 46.10 kJ mol^{-1}. The E_a for methanol oxidation visible by bio-Pt NPs is getting smaller as the potential, E increases from 0.35, 0.40, 0.45 to 0.60 V as shown in Table 4. This indicates a higher intrinsic activity and a faster charge transfer process by the bio-Pt NPs (Shafaei Douk et al., 2018b). A smaller E_a leads to faster charge transfer on the catalyst surface. The E_a value calculated in this study obtained in the acidic medium corresponds to the reference Pt-based electrocatalyst values in the reference range of 36-86 kJ/mol^{-1}, as reported by Douk et al. (2018) for Pt-Ag/G bimetallic, Jing et al. (2013) for Pt/C, Velázquez-Palenzuela et al. (2011) for PtRu, Colmati et al. (2006) for Pt and Aramata et al. (1988) for Pt. This indicates the presence of higher intrinsic activity and a faster charge transfer process by the bio-Pt NPs (Shafaei Douk et al., 2018a).

Table 4. Activation energy for methanol oxidation reaction in acidic medium at different potentials.

Electrocatalysts	**Activation energy, E_a (kJ mol^{-1}) at different potential (V)**			
	0. 35	0.40	0.45	0.60
Bio-Pt NPs	46.10	44.61	37.17	4.87
Commercial Pt black	11.78	13.77	15.35	6.90

Yet in contrast to commercial Pt black, where at the same potential, the E_a increases from 0.35 V to 0.45 V and then decreases when it reaches 0.60 V. This is likely due to the kinetic rate of the oxidation reaction occurring slowly compared to the bio-Pt NPs. If observed to be related to the onset potential, E_{onset}, i.e., the onset of the oxidation reaction, occurs in which, E_{onset} for commercial Pt black shifts to a more positive potential value than bio-Pt NPs, which E_{onset} shifts to a more negative potential as the reaction temperature increases. The more negative the E_{onset} potential means the faster for a methanol oxidation reaction to occur.

3.2.6 Effect of electrocatalyst loading on MOR

Electrocatalyst loading is another OFAT parameter significantly affecting the current density response. As shown in Fig. 9a and 9b, when the bio-inspired Pt NPs loading increased from 1.5 mg to 2.0 mg, the current density, j_p of MOR was remarkably enhanced; however, a further increase in electrocatalyst loading to 2.5 mg deteriorated MOR performance, as can be seen from a large drop of j_p. This is possible because high electrocatalyst loading causes particle aggregation and reduces the surface area for the oxidation reaction, contributing to the dispersion of undesirable reactants and products. Therefore, the best results were obtained at an electrocatalyst loading of 2.0 mg with a current density of 397.35 mA mg^{-1}_{Pt}.

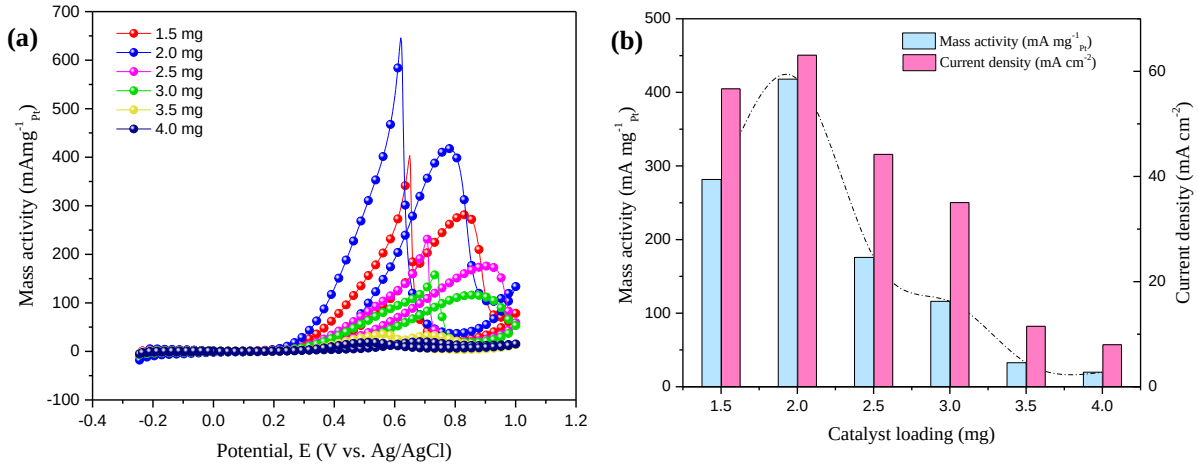

Fig. 9. (a) CV voltammogram of bio-Pt NPs electrocatalyst at varied catalyst loading, and (b) performance comparison graph.

3.3 Process optimization: Statistical analysis of developed model using RSM

3.3.1 Analysis of regression model

The electrocatalytic performance of MOR by the bio-inspired Pt NPs was modeled using RSM by CCD design. Table 5 shows the experimental design, predicted values, and actual values of the current density (mA/mg_{Pt}) of MOR produced by the bio-inspired Pt NPs. The experimental data was subject to multiple regression analysis to acquire a second-order polynomial equation from analysis of variance (ANOVA) by assessing the statistical significance of the model equation. The developed regression model is evaluated by

630 calculating the value of the coefficient of determination (R^2), analysis of variance (ANOVA),
631 F-value and P-value which are significant, so that one can confirm the significance of each
632 experimental variable carried out (Zafari et al., 2019). Using regression techniques, the
633 experimental results are matched with a quadratic model. The second-order polynomial
634 model for current density (mA/mg_{Pt}) of MOR using electrocatalyst bio-inspired Pt NPs is
635 given by Eq. (15):

636 $y = +407.14 + 152.40X_1 + 62.06X_2 - 27.21X_3 + 5.86X_1X_2 + 7.65X_1X_3 - 4.65X_2X_3 + 40.10X_1^2$
637 $- 103.22X_2^2 + 10.66X_3^2$

638 Table 5. Experimental design matrix, actual and predicted value of responses of current
639 density for MOR.

Run	**Variables**			**Response (Y) Current density (mA/mg_{Pt})**	
	X_1: Concentration of bio-Pt NPs	**X_2: Electrocatalyts loading (mg)**	**X_3: CH_3OH concentration (M)**	**Actual**	**Predicted**
1	0.5	2	1.5	230.42	294.84
2	0.5	2.5	1	309.15	297.98
3	1.5	2.5	1	590.69	599.21
4	0.5	2.5	2	230.36	218.97
5	1	2	1.5	458.87	407.14
6	0.5	1.5	2	135.90	115.87
7	1	2	1.5	382.80	407.14
8	1.5	1.5	1	454.18	454.06
9	1	2	1.5	455.67	407.14
10	1.5	1.5	2	424.58	424.25
11	0.5	1.5	1	198.11	176.29
12	1	2.5	1.5	362.26	365.98
13	1	1.5	1.5	199.56	241.86
14	1.5	2.5	2	540.49	550.80
15	1	2	1.5	446.49	407.14
16	1.5	2	1.5	618.03	599.64
17	1	2	2	369.15	390.59
18	1	2	1.5	382.80	407.14
19	1	2	1	420.43	445.01
20	1	2	1.5	408.25	407.14

640

641 ANOVA is used to determine the significant values of F, P-value, and R^2 in the
642 interaction between independent variables, as interpreted in Table 6. The quality of the

selected quadratic model is determined by the coefficient of determination (R^2), and the predicted R^2 for the selected quadratic model was 0.9500, which indicates that the model exhibits 95.00% variability and confirms its consistency in achieving the predicted values. Furthermore, the model recorded a predicted R^2 value of 0.7899, which is in reasonable agreement with the adjusted R^2 (0.9050), confirming a good relationship between the predicted and adjusted values of the current density percentage suggested by the model. The ANOVA result indicates a statistically significant quadratic model at a 95% confidence interval owing to its low p-value (≤ 0.0001) and a high F-value for the current density response (mA/mg_{Pt}) of 21.11. An F-value of 21.11 describes only a 0.01 % chance that a large F-value could occur due to interference. A higher F value and a lower P value mean the significance of the regression model is high (Idris et al., 2020).

The predicted model gave a standard deviation value of 40.54 and 0.9500 for the standard deviation and R^2 value, which indicated that 95 % of the total variation in response could be explained by the model. In addition, this model has sufficient accuracy because the ratio of signal to noise is 16.878, which is ≥ 4. Therefore, the presented model is consistent with the experimental data and can be used to predict the next response. Furthermore, the adequacy of this second-order polynomial model is also confirmed by a non-significant lack of fit. This shows that the model is a good fit for all the data. This result indicates that the model accurately and appropriately predicts the data in the experimental region. In conclusion, all parameters tested from the bio-inspired Pt NPs utilization as electrocatalyst in MOR are significant for the current density response (mA/mg_{Pt}).

Table 6. ANOVA analysis for response function y which is current density (mA/mg_{Pt}) for methanol oxidation activity.

Source	**Sum of square**	**df**	**Mean square**	**F-value**	**p-value (Prob > F)**
Model	3.121E+005	9	34679.03	21.11	< 0.0001 (significant)
X_1: Bio-Pt NPs	2.323E+005	1	2.323E+005	141.35	< 0.0001

concentration					
X_2: Electrocatalyst loading	38516.57	1	38516.57	23.44	0.0007
X_3: CH_3OH concentration	7402.52	1	7402.52	4.51	0.0598
X_1X_2	275.00	1	275.00	0.17	0.6911
X_1X_3	468.30	1	468.30	0.29	0.6051
X_2X_3	172.94	1	172.94	0.11	0.7523
X_1^2	4421.88	1	4421.88	2.69	0.1319
X_2^2	29299.96	1	29299.96	17.83	0.0018
X_3^2	312.55	1	312.55	0.19	0.6720
Residual	16431.62	10	1643.16		
Lack-of-fit	10077.41	5	2015.48	1.59	0.3126 (not significant)
Pure error	6354.21	5	1270.84		
Correlation total	3.285E+005	19			
Standard deviation	40.54		R^2	0.9500	
Mean	380.91		Adj R^2	0.9050	
			Pred R^2	0.7899	

Fig. 10a shows the plot of the predicted value against the experimental value of the current density (mA/mg_{Pt}), which shows a high correlation between the actual value and the predicted value because the data distribution is relatively close to the 45º diagonal angle (Balajii and Niju, 2019). The percentage of normal probability of the residual plot obtained by the model is given in Fig. 10b. Studentized residuals are used to check the hypothesized intimacy of variance by plotting residuals against normal probability values. The data spread homogeneously lie on the straight line, indicating that the residual follows the normal distribution and has appropriate normal error terms, showing the appropriateness of the model for this study (Kivrak et al., 2018). Fig. 10c is a plot of residuals against predictions showing a random distribution of points on the plot, showing that there is a constant range of residuals, and no unusual patterns are detected. This shows that the proposed quadratic model is adequate.

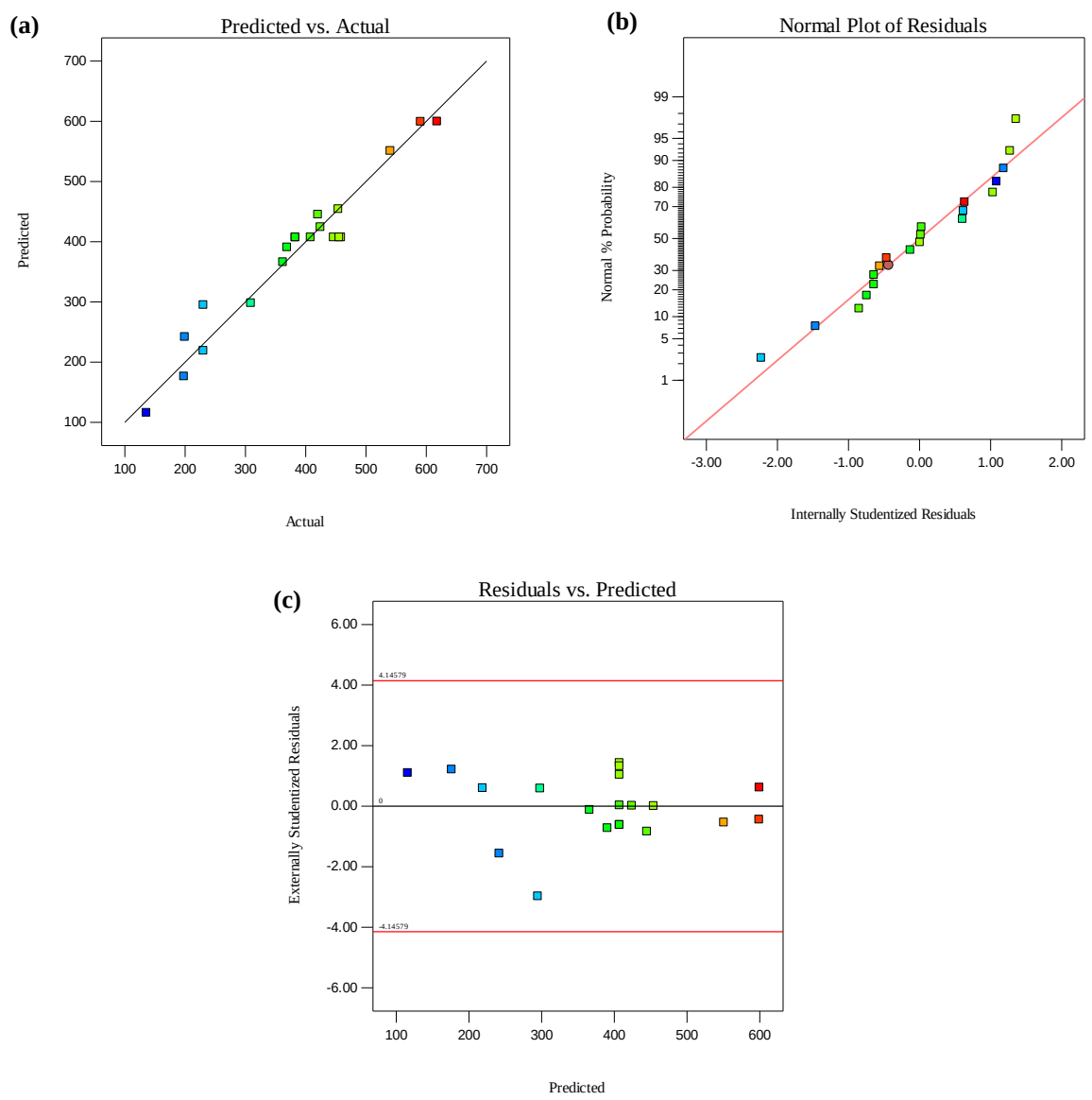

Fig. 10. Correlation evaluation of RSM predictions for current density (mA/mg_{Pt}) produced by bio-Pt NPs electrocatalysts (a) Predicted versus actual plot, (b) Normal plot of residuals, and (c) Residual versus predicted plot.

3.3.2 Parametric effect of process variables on current density response

Contour 2D plots and surface 3D plots represent the interaction effects between process parameters and responses. In this second-order polynomial equation plot, two parameters are manipulated within a defined experimental range and one parameter is kept constant. Fig. 11a and 11b represent the contour 2D plot and surface 3D plot explaining the interaction of parametric effects between X_1: Bio-Pt NPs concentration (mM) and X_2: electrocatalyst

loading (mg) on the current density response (mA/mg_{Pt}). The X_1 parameter varies from 0.5 to 1.5 mM and the X_2 parameter from 1.5 to 2.5 mg, while, the X_3 parameter is constant at a central level of 1.5 M. As the concentration of the bio-inspired Pt NPs increases, the current density reaches an optimum at a maximum concentration of 1.5 mM. Contrary to the electrocatalyst loading, the current density increases when it reaches the optimum value at 2.0 mg electrocatalyst loading, then decreases as the factor increases. As can be seen in the 2D contour plots and 3D surface plots, the red area represents the area of optimal response values of high current density.

From the effect of X_1X_2 interaction at a low level of both X_1 and X_2, the graph shows a low current density (≤ 200 mA/mg_{Pt}). This is because the availability of low active sites and the low surface area of the electrocatalyst cause the amount of methanol to adsorp on the surface of the electrocatalyst to be insufficient (Balajii and Niju, 2019). However, the current density continues to rapidly increase when the X_1 factor is increased up to 1.5 mM. The presence of many active sites and the availability of a high and sufficient surface area, provide a reaction path between the reactants that is also high and promotes the activity of the methanol oxidation reaction, and reaches a maximum value of 618.034 mA/mg_{Pt}. However, at the same time, when the X_2 factor is increased to 2.5 mg, the current density decreases. This can be related to the increase in electrocatalyst loading causing particle agglomeration and then reducing the total surface area of the electrocatalysts, and the electrocatalyst loading value of 2.0 mg is the ideal amount of electrocatalyst loading for MOR activity to occur.

Fig. 11c and 11d illustrate the interaction effect between the parameters of bio-Pt NPs concentration (X_1) and CH_3OH concentration (X_3) at the electrocatalyst loading setting of 2 mg. Based on the 2D and 3D plots shown in Fig. 11c and 11d, it shows that the current density increases with increasing bio-Pt NPs concentration from 0.5 to 1.5 mM and CH_3OH concentration from 1.0 to 1.5 M and then remains relatively constant. This trend is also

observed to be strongly influenced by the effect of the bio-Pt NPs concentration parameter, as shown in Fig. 11a. Statistically, of the three selected parameters, the bio-Pt NPs concentration (X_1) term is the most crucial parameter to the methanol oxidation current density response because it shows the highest F-value (141.35) and low p-value (<0.0001). This phenomenon can be attributed to the difference in the number of reactant particles between the solid (electrocatalyst) and liquid (methanol) phases (Yang et al., 2020). The higher the concentration of bio-Pt NPs in the methanol solution, the higher the chance of the collision frequency between the reactant particles occurring, and the reaction rate also increases. However, when the concentration of CH_3OH increases further, the dynamic equilibrium is already reached because the adsorption on the active site of the electrocatalyst is saturated and the reaction rate becomes constant.

Fig. 11e and 11f show the interactive effect between parameters X_2: electrocatalyst load (mg) and X_3: methanol concentration, while the bio-Pt NPs concentration remains at the final level (1.5 mM). A graph of the X_2X_3 interaction shows a modest increase in current density from 454.179 mA/mg_{Pt} to 618.034 mA/mg_{Pt} as X_2 is increased from 1.5 mg to 2.0 mg, and then a slight decline to 590.689 mA/mg_{Pt} as X_2 is further increased. Similarly, the same pattern is observed when the X_3 parameter is increased, the current density increases from 1.0 M to 1.5 M. However, when the methanol concentration is increased, the current density tends to decrease slightly due to the coverage of the active site by carbonaceous intermediate species generated during the methanol oxidation process, which impedes the diffusion of reactants and worsens, resulting in electrocatalyst poisoning (Amani et al., 2015). In Fig. 11f, the 3D plot with a flat surface indicates that the combination of the X_2X_3 parameters has a minimal effect on the current density result. In light of the ANOVA results, the bio-Pt NPs concentration is the most significant parameter, followed by electrocatalyst

loading and, finally, CH_3OH concentration in response to the current density (mA/mg_{Pt}) of MOR.

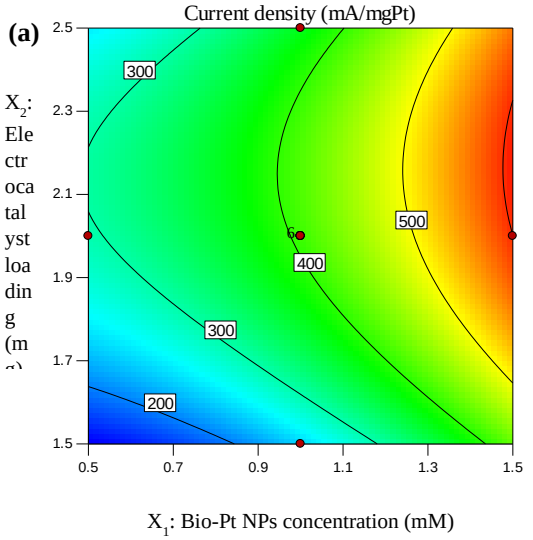

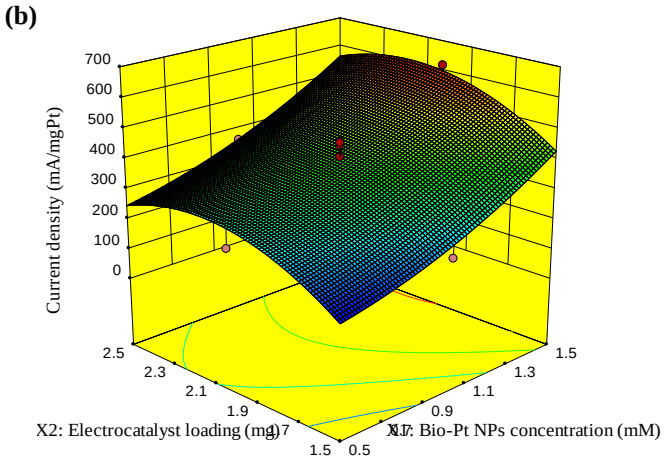

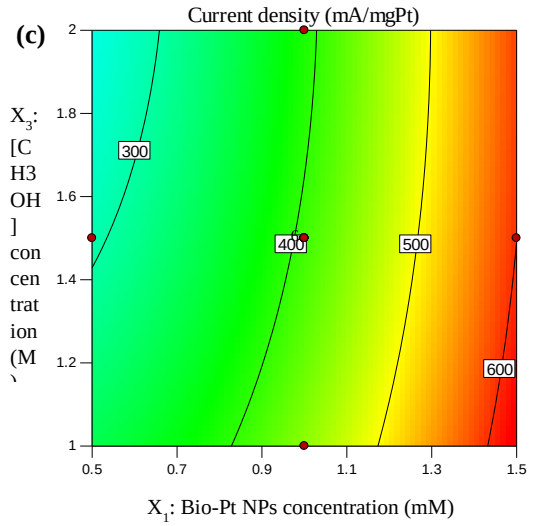

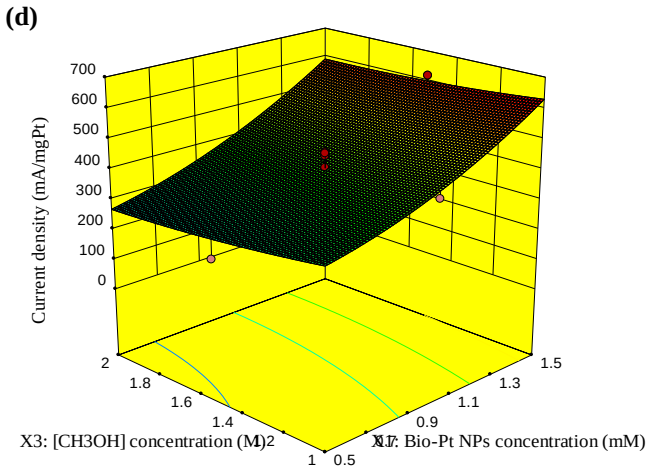

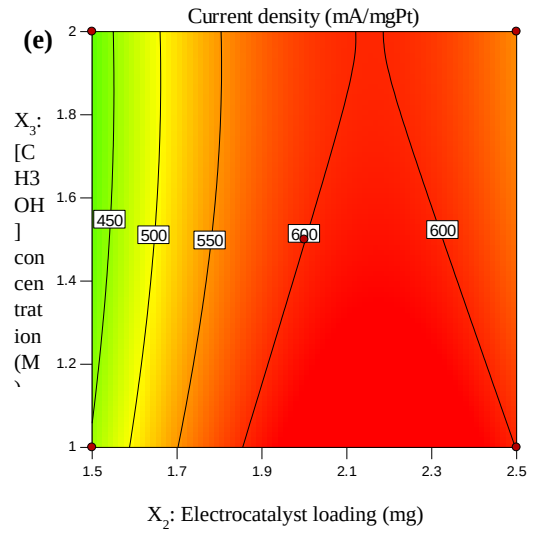

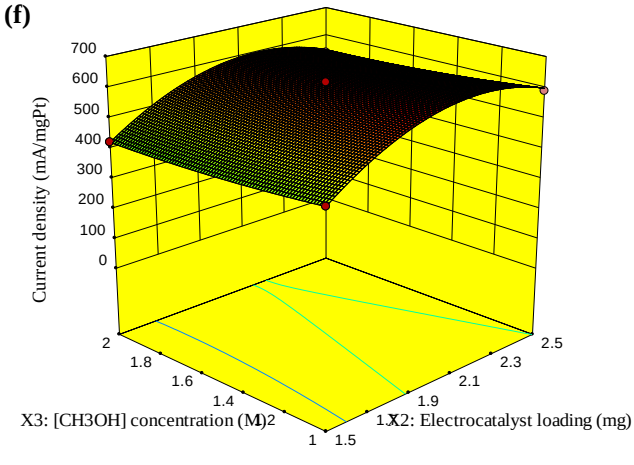

Fig. 11. Parametic effect for current density (mA/mg$_{Pt}$) of methanol oxidation reaction from electrocatalyst bio-Pt NPs (a – b) bio-Pt NPs concentration *vs*. electrocatalyst loading, (c - d) bio-Pt NPs concentration *vs*. methanol concentration and (e – f) Electrocatalyst loading *vs*. methanol concentration.

3.3.3 Validation of optimum process parameters

The optimal conditions for achieving the maximum current density for methanol oxidation activity are achieved by performing numerical optimization analysis in the CCD RSM design provided by Design-Expert software. From the desirability function, ideal values can be obtained for three parameters, including bio-inspired Pt NPs concentration, CH_3OH concentration, and electrocatalyst loading to ensure the highest selectivity of the maximum power density (mA/mg$_{Pt}$). The model predicts the maximum current density found at ideal conditions: 1.5 mM bio-Pt NPs concentration, 2.14 mg electrocatalyst loading, and 1.05 M CH_3OH concentration with a desirability of 1.000, as indicated in Fig. 12a and 12b. Validation experiments were performed in triplicate at the stated conditions and presented in Fig. 13a difference between the experimental result and the prediction of the current density response (mA/mgPt) is used to calculate the error and is shown in Table 7. The experimental result obtained 640.11 mA/mg$_{Pt}$ in average with only 0.63% error for the current density response results (mA/mg$_{Pt}$) is almost sufficient to confirm the reliability of the developed model.

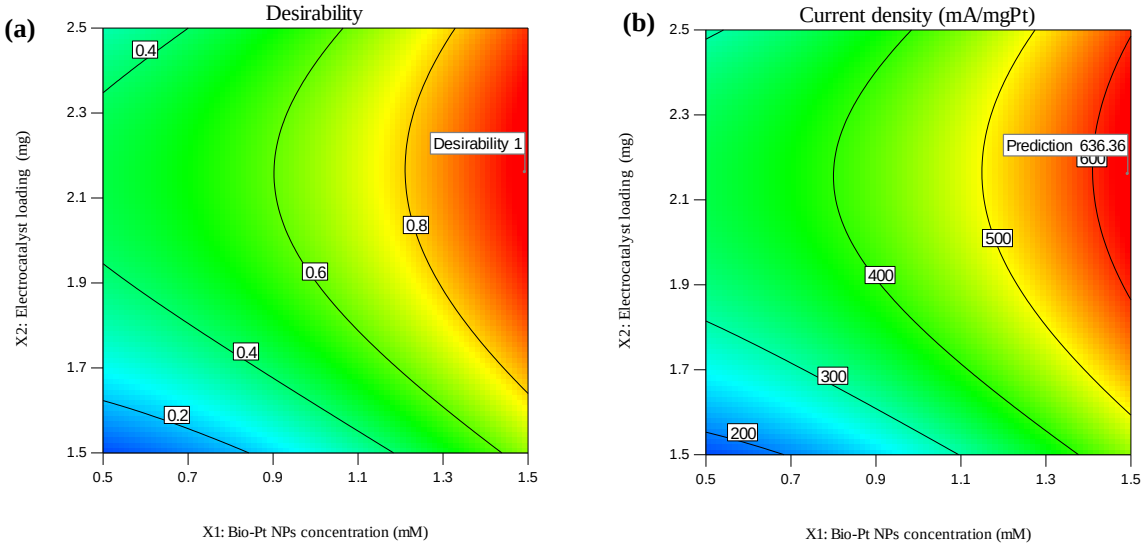

Fig. 12 The 2D contour plot for the numerical optimization of the optimum selection with a range of bio-Pt NPs concentration, CH_3OH concentration and electrocatalyst loading (a) numerical optimization desirability, and (b) expected optimal selection from numerical optimization.

Table 7. Validation test from numerizal optimization for the current density model.

Experiments	Bio-Pt NPs concentration (mM)	Electrocatalyst (mg)	CH_3OH concentration (M)	Current density (mA/mg_{Pt})		Error (%)
				Experiment	Prediction	
1	1.5	2.14	1.0	640.25	636.07	
2	1.5	2.14	1.0	656.27	636.07	
3	1.5	2.14	1.0	623.80	636.07	
Average				640.11	636.07	0.63

The results from the validation experiments of the optimal bio-inspired Pt NPs are compared with several other Pt-based electrocatalyst studies and are tabulated in Table 8 and illustrated in Fig. 13b. Compared to other electrocatalysts, bio-inspired Pt NPs performed best in the comparative study, with the highest current density values (Chen et al., 2016), (Yao et al., 2021), (Li et al., 2020), (Li et al., 2016), (Xiong et al., 2017), (Lu et al., 2018), (Yang et al., 2021), (Ren et al., 2019), (Y. Chen et al., 2020), (Shuli Yin,‡ Rajaiah Dhilip Kumar,‡ Hongjie Yu, Chunjie Li, Ziqiang Wang, You Xu, Xiaonian Li, Liang Wang, 2019), (Fu et al., 2016). As such, this bio-inspired Pt NPs as anode electrocatalyst is therefore very relevant from the perspective of performance and economics since it can reduce the cost of electrocatalyst preparation, is environmentally friendly, is an effortless technique, and is capable of generating a higher current density than existing electrocatalysts developed from various synthesis processes.

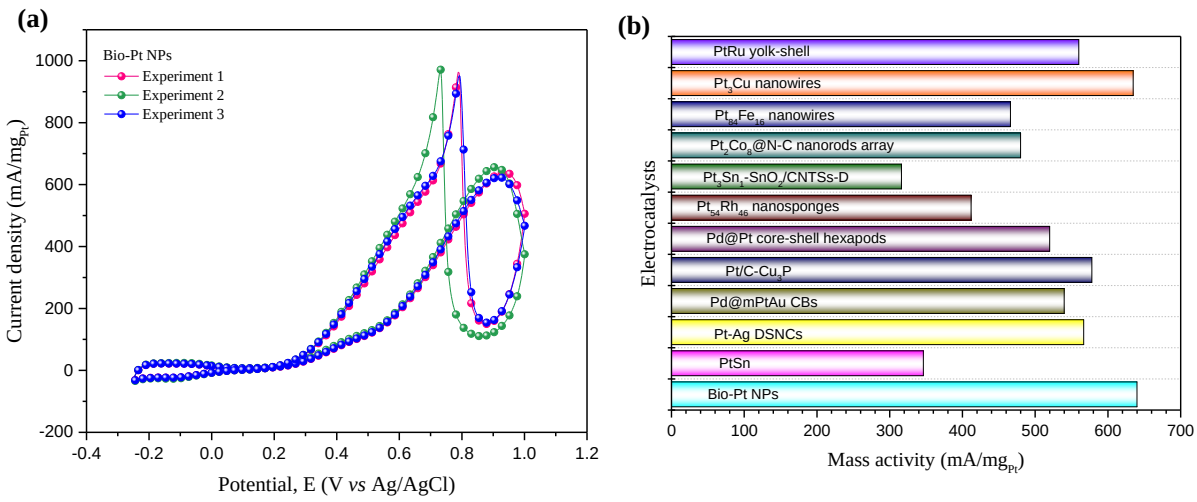

Fig. 13. (a) CV voltammogram of current density model validation experiment (mA/mg$_{Pt}$) of bio-Pt NPs and (b) comparison with previous reported Pt-based electrocatalyst in acidic MOR.

Table 8. Comparison of current density (mA/mg$_{Pt}$) of unsupported Pt-based electrocatalysts in 0.5 M H_2SO_4 + 1.0 M CH_3OH.

References	**Electrocatalyst and the morphologies**	**Synthesis methods**	**ECSA (m^2/g Pt)**	**Mass activity (mA mg_{Pt}^{-1})**
This study after optimization	Bio-Pt NPs	One-pot biosynthesis using plant extract	94.78	640.11
This study before optimization	Bio-Pt NPs	One-pot biosynthesis using plant extract	77.16	398.20
Chen et al. (2016)	Cubic PtSn	Coreduction	17.1	346.3
Yao et al. (2021)	Pt-Ag DSNCs	Hydrothermal	17.8	566.8
Li et al. (2020)	Pd@mPtAu CBs	Solvothermal	46.4	540.0
Li et al. (2016)	Pt/C-Cu_3P 50%	Conventional chemical reduction	-	578.02
Xiong et al. (2017)	Pd@Pt core-shell hexapods	Seed- mediated	6.3	520.0
Lu et al. (2018)	$Pt_{54}Rh_{46}$ nanosponge	Conventional chemical reduction	32.9	412.0
Yang et al. (2021)	Pt_3Sn_1-SnO_2/CNTs-D	Conventional chemical reduction	46.60	316.2
Ren et al. (2019)	Pt_2Co_8@N-C nanorods array	Galvanic replacement reaction	20.0	~480.0
Chen et al. (2020)	$Pt_{84}Fe_{16}$ nanowayar	Conventional chemical reduction	48.1	466
Fu et al.	Pt_3Cu wavy	Hydrothermal	20.3	634.78

(2016)	nanowires			
Yin et al. (2019)	PtRu *yolk-shell*	Conventional chemical reduction	30.8	560

3.4 Passive DMFC single cell performance

As a study component, bio-inspired Pt NPs were evaluated as anode electrodes in a passive single-cell DMFC to test their performance. Fig. 14 illustrated the polarization curve of the power density of passive DMFC for bio-inspired Pt NPs and commercial Pt black fed with 2 M CH_3OH. It was observed that the maximum power density of bio-inspired Pt NPs reached 5.70 mW cm^{-2} at a temperature of 25 ºC with a limiting current density of 81.61 mA cm^{-2} and an open circuit voltage (OCV) of 0.61 V. The single cell performance by the bio-inspired Pt NPs anode electrode seems satisfactory and is close to 86.62 % with the power density of the commercial Pt black anode electrode which recorded 6.58 mW cm^{-2} at a current density of 30.53 mA cm^{-2} at a temperature of 25 ºC. Nevertheless, the limiting current of the bio-Pt NPs electrode has been found to be higher, which is 81.61 mA cm^{-2}, in comparison to the limiting current of the commercial Pt black electrode (67.61 mA cm^{-2}). For further comparison, the DMFC single cell performances were also tested at operating temperatures of 80 and 100 ºC as shown in Fig. 14 and Table 9. The operating temperature of the passive DMFC influences cell performance. A rise in operating temperatures increase cell performance at maximum power density (P_{max}).

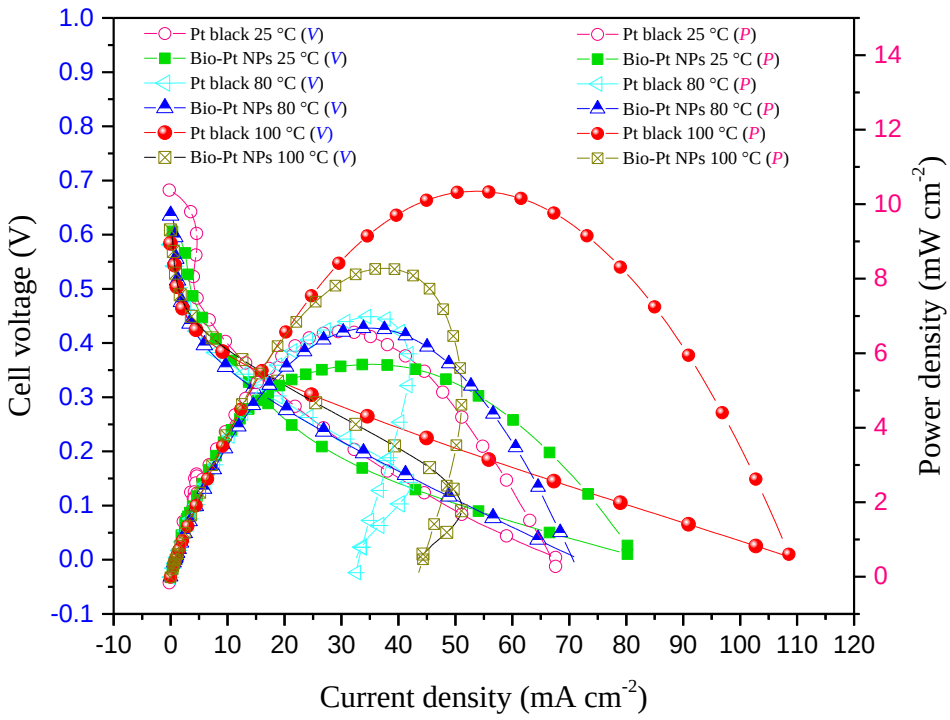

Fig. 14. Polarization curve of Current-Voltage (I-V) and current density of DMFC single cell performance for bio-Pt NPs and commercial Pt black at 2 M CH_3OH and varied temperatures (25, 80 and 100ºC).

The power density of bio-Pt NPs reaches 6.67 mW cm^{-2} at 80 ºC and almost 1.25 times that of 8.28 mW cm^{-2} at 100 °C. Meanwhile, commercial Pt black increased to reach 10.35 mW cm^{-2} at an operating temperature of 100 ºC. Several factors contribute to the increase in power density in single cell performance. First, increased temperature induces the kinetic reactions of both sides of the anode and cathode (MOR and ORR), thereby reducing the loss of activation during the discharging process (Pan et al., 2019). Second, as the operating temperature increases, concentration loss decreases. Higher temperatures facilitate the transport of reactants in the anolyte and catholyte (Pan et al., 2019). There is also an increase in the transport of cations penetrating the membrane. Consequently, this increased transport allows reactants to reach the active sites in the electrocatalyst layer more quickly, lowering the concentration loss rate since the lack of reactants is resolved. Finally, as the operating temperature escalates, the conductivity of the single cell will improve, reducing

ohmic losses (Li et al., 2009), (Pan et al., 2019). Comparing the bio-inspired Pt NPs to the commercial Pt black, the bio-inspired Pt NPs demonstrated satisfactorily comparable high current-voltage (IV) polarization curves for passive DFMC single cells and even outperformed previously reported Pt-based catalysts in single cell DMFC tests, as shown in Table 10. Specifically, the single cell performance tests conducted in passive mode cannot be compared to those conducted in active mode.

Table 9. Passive DMFC single-cell test assessment output.

Electrocatalysts	**OCV (V)**	**Maximum power density, P_{max} (mW cm^{-2})**	**Maximum current density, i_{max} (mA cm^{-2})**
Bio-Pt NPs 25 ºC	0.61	5.70	81.61
Pt black 25 ºC	0.68	6.58	67.61
Bio-Pt NPs 80 ºC	0.64	6.67	70.85
Pt black 80 ºC	0.58	6.99	42.02
Bio-Pt NPs 100 ºC	0.61	8.28	51.14
Pt black 100 ºC	0.58	10.35	108.56

Table 10. Comparison of passive DMFC single cell performance results with previous studies.

References	**Electrocatalyst**	**Synthesis methods**	**Power density (mW/cm^2)**
This study	Bio-inspired Pt NPs	One-pot biosynthesis using plant extract	5.70 (25 ºC), 6.67 (80 ºC), 10.35 (100 ºC)
Abdullah et al. 2018	PtRu/TiO_2-CNF	Conventional chemical reduction and high temperature pyrolisis at 600 ºC	3.8
Ramli et al. 2020	PtRu/CNC	Microwave polyol reduction and high temperature pyrolisis at 750 ºC	3.35
Amani et al. 2015	PtSn/C-PANI	Impregnation reduction	~ 4.0
Gharibi et al. 2013	Pt/C-PANI-PTSA	Impregnation reduction	2.5
Munjewar & Thombre 2019	PtRu/C	Commercial	4.227

4. CONCLUSION

The biosynthesis protocol was fine-tuned to deliver the bio-inspired Pt NPs to catalyze the methanol oxidation reaction for the first time efficiently. Bio-inspired Pt NPs have been found to have the highest catalytic activity among those synthesized using physiochemical techniques, possibly underpinned by the effect of organic biomolecular conjugations. The bio-inspired Pt NPs performance reaches a high current density of 581.50 mA mg_{Pt}^{-1} and a greater ECSA of 93.41 m^2 g^{-1}, in contrast to commercial Pt black (158.12 mA mg_{Pt}^{-1}/27.49 m^2 g^{-1}). The Bio-$Pt_{1.5}$ showed a lower Tafel slope, 179 mV dec^{-1} with exchange current, α = 0.33, than that of commercial Pt black (233 mV dec^{-1} and α = 0.25), meaning improved intrinsic kinetic activity. The RSM framework through the CCD model was used to optimize and maximize the current density of MOR by the bio-inspired Pt NPs. The effect of the bio-inspired Pt NPs concentration gave the most significant results on the current density (mA/mg_{Pt}) response and influenced the formation of the anisotropic morphological structure of bio-inspired Pt NPs. The current density of bio-inspired Pt NPs leverages 640.11 mA/mg_{Pt} at the optimum parameter conditions of 1.5 mM bio-Pt NPs concentration, 1.05 M CH_3OH concentration, and 2.14 mg of the electrocatalyst. Finally, the single-cell performance test of passive DMFC by bio-inspired Pt NPs yielded power densities, *P*max of 5.70, 6.67, and 8.28 mW cm^{-2} at temperature of 25, 80, and 100 ºC. Therefore, this study demonstrates that a biosynthesis-based plant extract-modified Pt NPs catalyst can improve electrocatalytic performance and control reaction chemistry in electrochemical reactions, such as MOR, at a meager cost and in a sustainable manner, making it an ideal option for anode electrodes in DMFC.

ACKNOWLEDGEMENTS

Thanks to the Ministry of Education (MOE) Malaysia and the Universiti Kebangsaan Malaysia for supporting this project under DIP-2021-028 and Sunway University under sponsorship GRTIN-IGS(02)-RCNMET-05-2023.

Credit Author Statement

Nurul Atiqah Izzati Md Ishak: Writing - original draft, Methodology, Investigation, Formal analysis, Resources. Siti Kartom Kamarudin: Conceptualization, Methodology, Validation, Supervision, Project administration, Funding acquisition. Muliani Mansor: Conceptualization and Validation. Norilhamiah Yahya: Conceptualization. Raihana Bahru: Copceptualization. Saidur Rahman: Conceptualization.

REFERENCES

Abdullah, N., Kamarudin, S.K., 2018. Novel Anodic Catalyst Support for Direct Methanol Fuel Cell : Characterizations and Single-Cell Performances. Nanoscale Res. Lett. 1–13.

Abdullah, N., Saidur, R., Zainoodin, A.M., Aslfattahi, N., 2020. Optimization of electrocatalyst performance of platinum–ruthenium induced with MXene by response surface methodology for clean energy application. J. Clean. Prod. 277, 123395. https://doi.org/10.1016/j.jclepro.2020.123395

Amani, M., Kazemeini, M., Hamedanian, M., Pahlavanzadeh, H., Gharibi, H., 2015. Investigation of Methanol Oxidation on a Highly Active and Stable Pt-Sn Electrocatalyst Supported on Carbon–Polyaniline Composite for Application in a Passive Direct Methanol Fuel Cell. Mater. Res. Bull. https://doi.org/10.1016/j.materresbull.2015.02.053

Amin, R.S., Abdel Hameed, R.M., El-Khatib, K.M., El-Abd, H., Souaya, E.R., 2012. Effect of preparation conditions on the performance of nano PtCuO/C electrocatalysts for methanol electro-oxidation. Int. J. Hydrogen Energy 37, 18870–18881. https://doi.org/10.1016/j.ijhydene.2012.10.009

Aramata, A., Kodera, T., Masuda, M., 1988. Electrooxidation of methanol on platinum bonded to the solid polymer electrolyte, Nafion. J. Appl. Electrochem. 18, 577–582. https://doi.org/10.1007/BF01022253

Balajii, M., Niju, S., 2019. A novel biobased heterogeneous catalyst derived from Musa acuminata peduncle for biodiesel production – Process optimization using central composite design. Energy Convers. Manag. 189, 118–131. https://doi.org/10.1016/j.enconman.2019.03.085

Chen, L., Liang, X., Li, X., Pei, J., Lin, H., Jia, D., Chen, W., Wang, D., Li, Y., 2020. Promoting electrocatalytic methanol oxidation of platinum nanoparticles by cerium modification. Nano Energy 73, 104784. https://doi.org/10.1016/j.nanoen.2020.104784

Chen, Q., Yang, Y., Cao, Z., Kuang, Q., Du, G., Jiang, Y., Xie, Z., Zheng, L., 2016. Excavated Cubic Platinum–Tin Alloy Nanocrystals Constructed from Ultrathin Nanosheets with Enhanced Electrocatalytic Activity. Angew. Chemie - Int. Ed. 55, 9021–9025. https://doi.org/10.1002/anie.201602592

Chen, W., Xue, J., Bao, Y., Feng, L., 2020. Surface engineering of nano-ceria facet dependent coupling effect on Pt nanocrystals for electro-catalysis of methanol oxidation reaction. Chem. Eng. J. 381, 122752. https://doi.org/10.1016/j.cej.2019.122752

Chen, Y., Liu, X., Sun, Y.-D., Yin, X., Jia, C., Ma, M., 2020. Enhanced Methanol Electrooxidation over Defect-rich Pt-M (M = Fe, Co, Ni) Ultrathin Nanowires. Energy & Fuels 34, 10078–10086. https://doi.org/10.1021/acs.energyfuels.0c01850

962 Cheng, H., Xia, J., Wang, M., Wang, C., Gui, R., Cao, X., Zhou, T., Zheng, X., Chu, W., Wu,
963 H., Xie, Y., Wu, C., 2022. Surface Anion Promotes Pt Electrocatalysts with High CO
964 Tolerance in Fuel-Cell Performance. J. Am. Chem. Soc. Am. Chem. Soc. 144, 22018–
965 22025. https://doi.org/10.1021/jacs.2c09147

966 Colmati, F., Antolini, E., Gonzalez, E.R., 2006. Effect of temperature on the mechanism of
967 ethanol oxidation on carbon supported Pt, PtRu and Pt3Sn electrocatalysts. J. Power
968 Sources 157, 98–103. https://doi.org/10.1016/j.jpowsour.2005.07.087

969 Darabi, R., Alown, F.E.D., Aygun, A., Gu, Q., Gulbagca, F., Altuner, E.E., Seckin, H.,
970 Meydan, I., Kaymak, G., Sen, F., Karimi-Maleh, H., 2023. Biogenic platinum-based
971 bimetallic nanoparticles: Synthesis, characterization, antimicrobial activity and
972 hydrogen evolution. Int. J. Hydrogen Energy 48, 21270–21284.
973 https://doi.org/https://doi.org/10.1016/j.ijhydene.2022.12.072

974 Dauthal, P., Mukhopadhyay, M., 2016. Noble Metal Nanoparticles: Plant Mediated
975 Synthesis, Mechanistic Aspects of Synthesis and Applications. Ind. Eng. Chem.
976 Reseacrh. https://doi.org/10.1021/acs.iecr.6b00861

977 Derlacki, Z.J., Easteal, A.J., Edge, A.V.J., Woolf, L.A., Roksandic, Z., 1985. Diffusion
978 coefficients of methanol and water and the mutual diffusion coefficient in methanol-
979 water solutions at 278 and 298 K. J. Phys. Chem. 89, 5318–5322.
980 https://doi.org/10.1021/j100270a039

981 Ding, J., Hu, W., Ma, L., Gan, M., Xie, F., Zhan, W., Lu, W., 2021. Facile construction of
982 mesoporous carbon enclosed with NiCoPx nanoparticles for desirable Pt-based catalyst
983 support in methanol oxidation. J. Power Sources 481, 1–9.
984 https://doi.org/10.1016/j.jpowsour.2020.228888

985 Ekrami-Kakhki, M.S., Naeimi, A., Donyagard, F., 2019. Pt nanoparticles supported on a
986 novel electrospun polyvinyl alcohol-CuO–Co3O4/chitosan based on Sesbania sesban
987 plant as an electrocatalyst for direct methanol fuel cells. Int. J. Hydrogen Energy 44,
988 1671–1685. https://doi.org/10.1016/j.ijhydene.2018.11.102

989 Eris, S., Daşdelen, Z., Sen, F., 2018. Enhanced electrocatalytic activity and stability of
990 monodisperse Pt nanocomposites for direct methanol fuel cells. J. Colloid Interface Sci.
991 513, 767–773. https://doi.org/10.1016/j.jcis.2017.11.085

992 Fu, G., Yan, X., Cui, Z., Sun, D., Xu, L., Tang, Y., Goodenough, J.B., Lee, J.M., 2016.
993 Catalytic activities for methanol oxidation on ultrathin CuPt3 wavy nanowires
994 with/without smart polymer. Chem. Sci. 7, 5414–5420.
995 https://doi.org/10.1039/c6sc01501h

996 Fuku, X., Modibedi, M., Matinise, N., Mokoena, P., Xaba, N., Mathe, M., 2019. Single step
997 synthesis of bio-inspired NiO/C as Pd support catalyst for dual application: Alkaline
998 direct ethanol fuel cell and CO 2 electro-reduction. J. Colloid Interface Sci. 545, 138–
999 152. https://doi.org/10.1016/j.jcis.2019.03.030

1000 Gharibi, H., Amani, M., Pahlavanzadeh, H., Kazemeini, M., 2013. Investigation of carbon
1001 monoxide tolerance of platinum nanoparticles in the presence of optimum ratio of doped
1002 polyaniline with para toluene sulfonic acid and their utilization in a real passive direct
1003 methanol fuel cell. Electrochim. Acta 97, 216–225.
1004 https://doi.org/10.1016/j.electacta.2013.01.121

1005 Guo, Y., Gao, Y., Li, X., Zhuang, G., Wang, K., Zheng, Y., Sun, D., Huang, J., Li, Q., 2019.

Catalytic benzene oxidation by biogenic Pd nanoparticles over 3D-ordered mesoporous CeO 2. Chem. Eng. J. 362, 41–52. https://doi.org/10.1016/j.cej.2019.01.012

Hasran, U.A., Kamarudin, S.K., Daud, W.R.W., Majlis, B.Y., Mohamad, A.B., Kadhum, A.A.H., Ahmad, M.M., 2013. Optimization of hot pressing parameters in membrane electrode assembly fabrication by response surface method. Int. J. Hydrogen Energy 38, 9484–9493. https://doi.org/10.1016/j.ijhydene.2012.12.054

Huang, L., Han, Y., Zhang, X., Fang, Y., Dong, S., 2017. One-step synthesis of ultrathin PtXPb nerve-like nanowires as robust catalysts for enhanced methanol electrooxidation. Nanoscale 9, 201–207. https://doi.org/10.1039/c6nr07036a

Hui, L., Xue, Y., Xing, C., Liu, Y., Du, Y., Fang, Y., Yu, H., Zhang, C., He, F., Li, Y., 2022. Atomic alloys of nickel-platinum on carbon network for methanol oxidation. Nano Energy. https://doi.org/10.1016/j.nanoen.2022.106984

Idris, R., Chong, C.T., Asik, J.A., Ani, F.N., 2020. Optimization studies of microwave-induced co-pyrolysis of empty fruit bunches/waste truck tire using response surface methodology. J. Clean. Prod. 244, 118649. https://doi.org/10.1016/j.jclepro.2019.118649

Ishak, N.A.I.M., Kamarudin, S.K., Timmiati, S.N., Karim, N.A., Basri, S., 2020. Biogenic platinum from agricultural wastes extract for improved methanol oxidation reaction in direct methanol fuel cell. J. Adv. Res. 1–13. https://doi.org/10.1016/j.jare.2020.06.025

Javan, H., Asghari, E., Ashassi-Sorkhabi, H., 2019. Fabrication and electrochemical kinetics studies of reduced carbon quantum dots- supported palladium nanoparticles as bifunctional catalysts in methanol oxidation and hydrogen evolution reactions. Synth. Met. 254, 153–163. https://doi.org/10.1016/j.synthmet.2019.06.006

Jing, M., Jiang, L., Yi, B., Sun, G., 2013. Comparative study of methanol adsorption and electro-oxidation on carbon-supported platinum in acidic and alkaline electrolytes. J. Electroanal. Chem. 688, 172–179. https://doi.org/10.1016/j.jelechem.2012.10.028

Kamarudin, S.K., Hashim, N., 2012. Materials, morphologies and structures of MEAs in DMFCs. Renew. Sustain. Energy Rev. 16, 2494–2515. https://doi.org/10.1016/j.rser.2012.01.073

Karim, N.A., Kamarudin, S.K., Loh, K.S., 2017. Performance of a novel non-platinum cathode catalyst for direct methanol fuel cells. Energy Convers. Manag. 145, 293–307. https://doi.org/10.1016/j.enconman.2017.05.003

Kivrak, H., Sahan, T., Yurtcan, A.B., Cogenli, M.S., Caglar, A., Aktas, N., 2018. A novel Central Composite Design based response surface methodology optimization study for the synthesis of Pd/CNT direct formic acid fuel cell anode catalyst. Int. J. Hydrogen Energy 43, 11002–11011. https://doi.org/10.1016/j.ijhydene.2018.04.208

Li, C., Liu, S., Yin, S., Yu, H., Wang, Z., Xu, Y., Li, X., Wang, L., Wang, H., 2020. Facile preparation of Pt-based cage-bell structured nanoarchitectures for enhanced methanol oxidation electrocatalysis. Int. J. Hydrogen Energy 45, 2478–2485. https://doi.org/10.1016/j.ijhydene.2019.11.192

Li, M., Chang, Y., Han, G., Yang, B., 2011. Platinum nanoparticles supported on electrospinning-derived carbon fibrous mats by using formaldehyde vapor as reducer for methanol electrooxidation. J. Power Sources 196, 7973–7978.

https://doi.org/10.1016/j.jpowsour.2011.05.060

Li, M., Zhao, S., Han, G., Yang, B., 2009. Electrospinning-derived carbon fibrous mats improving the performance of commercial Pt/C for methanol oxidation. J. Power Sources 191, 351–356. https://doi.org/10.1016/j.jpowsour.2009.01.089

Li, R., Ma, Z., Zhang, F., Meng, H., Wang, M., Bao, X.Q., Tang, B., Wang, X., 2016. Facile Cu3P-C hybrid supported strategy to improve Pt nanoparticle electrocatalytic performance toward methanol, ethanol, glycol and formic acid electro-oxidation. Electrochim. Acta 220, 193–204. https://doi.org/10.1016/j.electacta.2016.10.105

Lu, Q., Huang, J., Han, C., Sun, L., Yang, X., 2018. Facile synthesis of composition-tunable PtRh nanosponges for methanol oxidation reaction. Electrochim. Acta 266, 305–311. https://doi.org/10.1016/j.electacta.2018.02.021

Ma, C., Liu, W., Shi, M., Lang, X., Chu, Y., Chen, Z., Zhao, D., Lin, W., Hardacre, C., 2013. Low loading platinum nanoparticles on reduced graphene oxide-supported tungsten carbide crystallites as a highly active electrocatalyst for methanol oxidation. Electrochim. Acta 114, 133–141. https://doi.org/10.1016/j.electacta.2013.10.034

Md Ishak, N.A.I., Kamarudin, S.K., Timmiati, S.N., Mohd Sauid, S., A Karim, N., Basri, S., 2023. Green synthesis of platinum nanoparticles as a robust electrocatalyst for methanol oxidation reaction: Metabolite profiling and antioxidant evaluation. J. Clean. Prod. 382, 135111. https://doi.org/10.1016/j.jclepro.2022.135111

Mittal, A.K., Chisti, Y., Banerjee, U.C., 2013. Synthesis of metallic nanoparticles using plant extracts. Biotechnol. Adv. 31, 346–356. https://doi.org/10.1016/j.biotechadv.2013.01.003

Mohamed, M.M., Khairy, M., Eid, S., 2016. Activity and stability studies of titanates and titanate-carbon nanotubes supported Ag anode catalysts for direct methanol fuel cell. J. Power Sources 304, 255–265. https://doi.org/10.1016/j.jpowsour.2015.11.054

Munjewar, S.S., Thombre, S.B., 2019. Effect of current collector roughness on performance of passive direct methanol fuel cell. Renew. Energy 138, 272–283. https://doi.org/10.1016/j.renene.2019.01.101

Nayak, S.P., Ventrapragada, L.K., Ramamurthy, S.S., Kiran Kumar, J.K., Rao, A.M., 2022. Green synthesis of a novel porous gold-curcumin nanocomposite for super-efficient alcohol oxidation. Nano Energy. https://doi.org/10.1016/j.nanoen.2022.106966

Nurul Atiqah Izzati Md Ishak, S.K. Kamarudin, Sharifah Najiha Timmiati, Nabila Karim, S.B., 2021. Enhanced performance of methanol oxidation reaction via green synthesis of platinum electro-catalyst from sugar cane bagasse. Int. J. Energy Res. 45, 7380–7403. https://doi.org/10.1002/er.6323

Ocampo-Restrepo, V.K., Calderón-Cárdenas, A., Lizcano-Valbuena, W.H., 2017. Catalytic Activity of Pt-Based Nanoparticles with Ni and Co for Ethanol and Acetaldehyde Electrooxidation in Alkaline Medium. Electrochim. Acta 246, 475–483. https://doi.org/10.1016/j.electacta.2017.06.014

Ojani, R., Hasheminejad, E., Raoof, J.B., 2015. Direct growth of 3D flower-like Pt nanostructures by a template-free electrochemical route as an efficient electrocatalyst for methanol oxidation reaction. Energy 90, 1122–1131. https://doi.org/10.1016/j.energy.2015.06.061

Pan, Z., Huang, B., An, L., 2019. Performance of a hybrid direct ethylene glycol fuel cell. Int. J. Energy Res. 43, 2583–2591. https://doi.org/10.1002/er.4176

Ramli, Z.A.C., Kamarudin, S.K., Basri, S., Zainoodin, A.M., 2020. The potential of novel carbon nanocages as a carbon support for an enhanced methanol electro-oxidation reaction in a direct methanol fuel cell. Int. J. Energy Res. 44, 10071–10086. https://doi.org/10.1002/er.5621

Ren, W., Zang, W., Zhang, H., Bian, J., Chen, Z., Guan, C., Cheng, C., 2019. PtCo bimetallic nanoparticles encapsulated in N-doped carbon nanorod arrays for efficient electrocatalysis. Carbon N. Y. 142, 206–216. https://doi.org/10.1016/j.carbon.2018.10.054

Selvanathan, V., Kumar, D., Mottakin, M., Islam, A., 2023. Aloe vera extract mediated hydrothermal synthesis of rose-like copper iron sulfide for efficient oxygen evolution reaction. J. Taiwan Inst. Chem. Eng. 151, 105131. https://doi.org/10.1016/j.jtice.2023.105131

Shaari, N., Kamarudin, S.K., 2018. Performance of crosslinked sodium alginate / sulfonated graphene oxide as polymer electrolyte membrane in DMFC application : RSM optimization approach. Int. J. Hydrogen Energy. https://doi.org/10.1016/j.ijhydene.2018.10.098

Shafaei Douk, A., Saravani, H., Noroozifar, M., 2018a. One-pot synthesis of ultrasmall Pt–Ag nanoparticles decorated on graphene as a high-performance catalyst toward methanol oxidation. Int. J. Hydrogen Energy 43, 7946–7955. https://doi.org/10.1016/j.ijhydene.2018.03.064

Shafaei Douk, A., Saravani, H., Noroozifar, M., 2018b. A fast method to prepare Pd-Co nanostructures decorated on graphene as excellent electrocatalyst toward formic acid oxidation. J. Alloys Compd. 739, 882–891. https://doi.org/10.1016/j.jallcom.2017.12.272

Shuli Yin,‡ Rajaiah Dhilip Kumar,‡ Hongjie Yu, Chunjie Li, Ziqiang Wang, You Xu, Xiaonian Li, Liang Wang, and H.W., 2019. Pt@Mesoporous PtRu Yolk−Shell Nanostructured Electrocatalyst for Methanol Oxidation Reaction. ACS Sustain. Chem. Eng. 7, 14867−14873.

Toghan, A., Khairy, M., Mokhtar, M., Amer, A.A., 2021. Synthesis of defect-impressive boron graphene as a remarkable electrocatalyst for methanol oxidation reaction. J. Mater. Res. Technol. 16, 362–372. https://doi.org/10.1016/j.jmrt.2021.12.001

Velázquez-Hernández, I., Estévez, M., Vergara-Castañeda, H., Guerra-Balcázar, M., Álvarez-Contreras, L., Luna-Bárcenas, G., Pérez, C., Arjona, N., Pool, H., 2020. Synthesis and application of biogenic gold nanomaterials with {1 0 0} facets for crude glycerol electro-oxidation. Fuel 279, 118505. https://doi.org/10.1016/j.fuel.2020.118505

Velázquez-Palenzuela, A., Centellas, F., Garrido, J.A., Arias, C., Rodríguez, R.M., Brillas, E., Cabot, P.L., 2011. Kinetic analysis of carbon monoxide and methanol oxidation on high performance carbon-supported Pt-Ru electrocatalyst for direct methanol fuel cells. J. Power Sources 196, 3503–3512. https://doi.org/10.1016/j.jpowsour.2010.12.044

Wo, A.A., Mokhtar, M., Syam, S.M., Khairy, M., 2023. Electrochimica Acta Extremely efficient methanol oxidation reaction performance : A highly active catalyst derived from different Mn 2-x O y. Electrochim. Acta 437, 141528.

https://doi.org/10.1016/j.electacta.2022.141528

Xiong, Y., Ma, Y., Li, J., Huang, J., Yan, Y., Zhang, H., Wu, J., Yang, D., 2017. Strain-induced Stranski-Krastanov growth of Pd@Pt core-shell hexapods and octapods as electrocatalysts for methanol oxidation. Nanoscale 9, 11077–11084. https://doi.org/10.1039/c7nr02638b

Xuewei Du, Shuiping Luo, Hongyu Du, Min Tang, Xiangdong Huang, P.K.S., 2013. Monodisperse and self-assembled Pt-Cu nanoparticles as an efficient electrocatalyst for methanol oxidation reaction. J. Mater. Chem. A.

Yahya, N., Kamarudin, S.K., Karim, N.A., Masdar, M.S., Loh, K.S., 2017. Enhanced performance of a novel anodic PdAu/VGCNF catalyst for electro-oxidation in a glycerol fuel cell. Nanoscale Res. Lett. 12. https://doi.org/10.1186/s11671-017-2360-x

Yang, F., Zhang, W., Wang, H., Gu, C., Lu, Y., Zhou, K., 2020. Determination of formaldehyde using a novel Pt-doped nano-sized sensitive material: Operating conditions optimization by response surface method. Anal. Chim. Acta 1132, 47–54. https://doi.org/10.1016/j.aca.2020.07.070

Yang, P., Li, Y., Chen, S., Li, J., Zhao, P., Zhang, L., Xie, Y., Fei, J., 2021. One-step synthesis in deep eutectic solvents of Pt3Sn1-SnO2 alloy nanopore on carbon nanotubes for boosting electro-catalytic methanol oxidation. J. Electroanal. Chem. 887, 115164. https://doi.org/10.1016/j.jelechem.2021.115164

Yao, W., Jiang, X., Li, M., Li, Y., Liu, Y., Zhan, X., Fu, G., Tang, Y., 2021. Engineering hollow porous platinum-silver double-shelled nanocages for efficient electro-oxidation of methanol. Appl. Catal. B Environ. 282, 1–10. https://doi.org/10.1016/j.apcatb.2020.119595

Zafari, R., Abdouss, M., Zamani, Y., 2019. Application of response surface methodology for the optimization of light olefins production from CO hydrogenation using an efficient catalyst. Fuel 237, 1262–1273. https://doi.org/10.1016/j.fuel.2018.10.074

Zhang, J., Chen, J., Jiang, Y., Zhou, F., Zhong, J., Wang, G., Kiani, M., Wang, R., 2016. Facile synthesis of flower-like platinum nanostructures as an efficient electrocatalyst for methanol electro-oxidation. J. Colloid Interface Sci. 479, 64–70. https://doi.org/10.1016/j.jcis.2016.06.050